Inhibition of Metabotropic Glutamate Receptor Subtype 1 Alters the Excitability of the Commissural Pyramidal Neuron in the Rat Anterior Cingulate Cortex after Chronic Constriction Injury to the Sciatic Nerve

Shi-Hao Gao, B.M., Lin-Lin Shen, B.M., Hui-Zhong Wen, Ph.D., Yan-Dong Zhao, Ph.D., Huai-Zhen Ruan, Ph.D.

ABSTRACT

Background: Inhibition of the metabotropic glutamate receptor subtype 1 in the anterior cingulate cortex has an analgesic effect during sustained nociceptive hypersensitivity. However, the specific changes in different subtypes of anterior cingulate cortex layer 5 pyramidal neurons, as well as the distinct effect of metabotropic glutamate receptor subtype 1 inhibition on different neuronal subtypes, have not been well studied.

Methods: Retrograde labeling combined with immunofluorescence, whole cell clamp recording, and behavioral tests combined with RNA interference were performed in a rat model of chronic constriction injury to the sciatic nerve.

Results: Commissural layer 5 pyramidal neurons (projecting to the contralateral cortex) existed in the anterior cingulate cortex. The voltage-gated potassium channel subunit 2–mediated current in these neurons were substantially reduced after chronic constriction injury (current densities at +30 mV for the sham, and chronic constriction injury neurons were [mean ± SD] 10.22 ± 3.42 pA/pF *vs.* 5.58 ± 2.71 pA/pF, respectively; n = 11; $P < 0.01$), which increased the spike width and fast afterhyperpolarization potential, resulting in hyperexcitability. Inhibition of metabotropic glutamate receptor subtype 1 alleviated the down-regulation of voltage-gated potassium channel subunit 2 currents (current density increased by 8.11 ± 3.22 pA/pF; n = 7; $P < 0.01$). Furthermore, knockdown of voltage-gated potassium channel subunit 2 current in the commissural neurons attenuated the analgesic effect of metabotropic glutamate receptor subtype 1 inhibition (n = 6 rats; $P < 0.05$).

Conclusions: The effect of metabotropic glutamate receptor subtype 1 inhibition on commissural anterior cingulate cortex layer 5 pyramidal neurons is likely different with the modification of previously studied hyperpolarization-activated/cyclic nucleotide-gated channel-dependent neurons but relies on the alteration of voltage-gated potassium channel subunit 2 currents. These results will contribute to a better understanding of the therapeutic role of metabotropic glutamate receptor subtype 1 in chronic pain. **(ANESTHESIOLOGY 2017; 127:515-33)**

THE persistent hyperactivity of the anterior cingulate cortex (ACC) is considered a key mechanism for the chronification of pain.[1–5] Elucidating how ACC hyperactivation affects other cortical regions and contributes to the persistent pain state may require understanding the mechanism of hyperexcitability on the output of the ACC. A primary source of output from the ACC occurs *via* the layer 5 pyramidal neurons (L5 PNs). Modulation of synaptic inputs to these neurons[6] and changes of their intrinsic properties[7] have been characterized in rodent models of peripheral nerve injury, indicating a pivotal participation of the hyperpolarization-activated cation nonselective current (I_h). However, in several neocortical regions, including the rat medial prefrontal cortex (mPFC), which is adjacent to the ACC, L5 PNs have distinct morphology and electrophysiology depending on their long-range projection targets.[8–11] The corticopontine neurons projecting subcortically to multiple targets, including the pontine nuclei, have I_h-dependent membrane properties, but the commissural neurons projecting to the contralateral cortex do not have these properties.

What We Already Know about This Topic

- Persistent hyperactivity of neurons in the anterior cingulate cortex, mediated in part by glutamatergic neurotransmission, contributes to the development of chronic pain.
- The output of the anterior cingulate cortex is mediated by two types of layer 5 pyramidal neurons, corticopontine fibers that project to subcortical nuclei and commissural fibers that project to the contralateral cortex. Hyperpolarization-activated/cyclic nucleotide-gated channels play an important role in the corticopontine neuronal activity, but the mechanisms by which commissural fibers are impacted by chronic injury are not known.

What This Article Tells Us That Is New

- In a rodent model of chronic constrictive injury, injury-induced hyperactivity of commissural fibers was associated with a reduction in voltage-gated potassium channel subunit 2–mediated current; metabotropic glutamate receptor inhibition produced an analgesic effect, restored voltage-gated potassium channel subunit 2 currents, and reduced hyperexcitability.
- The data support the notion that the analgesic efficacy of metabotropic glutamate receptor inhibition is in part mediated by reducing anterior cingulate cortex output to the contralateral cerebral cortex.

 Anesthesiology 2017; 127:515-33

<zdoi;10.1097/ALN.0000000000001654>

Therefore, it seems that ACC L5 PNs may also be divided into two subtypes, but the specific excitability changes in the different cell types, particularly the contralateral-projecting and I_h-independent neurons, still remain unknown during chronic pain, to the best of our knowledge.

The glutamatergic system has been shown to play a critical role in pain processing in the ACC,[12] and the metabotropic glutamate receptor subtype 1 (mGluR1) is of vital importance due to its therapeutic implications for chronic pain.[13–17] It has been shown that the sciatic nerve injury-induced dysfunction of cortical dendritic integration may be mGluR1 dependent,[6] and inhibition of mGluR1 changes the intrinsic property of I_h-positive ACC L5 PNs after peripheral nerve injury.[7] Nevertheless, the different subtypes of L5 PNs may respond diversely to the same neurotransmitter system, such as the noradrenergic, acetylcholinergic, dopaminergic, and serotoninergic systems.[9,18–20] Thus, exploring the specific role of mGluR1 on different cell types, particularly on contralateral-projecting neurons, will contribute to a better understanding of its therapeutic effect in chronic pain.

In the present study, we confirmed a subtype of ACC L5 PNs, which project to the contralateral ACC and exhibit little I_h. Thus, we investigated changes in the firing properties of these contralateral-projecting neurons under the condition of chronic constriction injury (CCI) to the sciatic nerve. We observed a voltage-gated potassium channel subunit 2 (Kv2)–related alteration of the action potential (AP) width and fast afterhyperpolarization (AHP; fAHP) potential after CCI, resulting in the hyperexcitability of these neurons. Moreover, we tested the effects of mGluR1 inhibition on Kv2 currents and the neuronal excitability of contralateral-projecting ACC L5 PNs, and we also evaluated whether these effects mediated the analgesia of mGluR1 antagonist.

Materials and Methods

Experimental Animals

Male Sprague–Dawley rats (200 to 240 g for immunofluorescence experiments and P28–P31 for whole cell recordings; Experimental Animal Center, Third Military Medical University, China) were maintained on a 12-h light/dark cycle with free access to food and water at a constant room temperature of 25° to 28°C. All efforts were made to minimize suffering and to reduce the number of animals used to the minimum required for statistical accuracy. Every experimental procedure was executed in accordance with the National Institutes of Health Guide for the Care and Use of Laboratory Animals and was approved by the Third Military Medical University Ethical Committee for Animal Research.

Submitted for publication November 7, 2016. Accepted for publication March 13, 2017. From the Department of Neurobiology, College of Basic Medical Science, Chongqing Key Laboratory of Neurobiology, Third Military Medical University, Chongqing, China (S.-H.G., H.-Z.W., Y.-D.Z., H.-Z.R.); and Department of Neurology, Daping Hospital, Third Military Medical University, Chongqing, China (L.-L.S.)

Chronic Constriction Injury

CCI to the sciatic nerve was performed according to the previous protocols[21,22] and followed the ethical guideline of the International Association for the Study of Pain regarding the use of laboratory animals.[23] Animals were randomized to the naïve, sham, or CCI group. After receiving anesthesia with 4% chloral hydrate (10 ml/kg, intraperitoneal), the right sciatic nerve of rats in the CCI group was exposed at the midthigh level, and four sterile 4–0 chromic gut ligatures were tied loosely around the nerve, 1.0 to 1.5 mm apart, proximal to its trifurcation. For sham surgery rats, the sciatic nerve was isolated without ligation. After CCI surgery, the affected hind paw was placed clumsily, and the toes were together and slightly ventroflexed. CCI rats walked with a definite limp, often raised the affected hind paw, and held it in a protected position,[22] which was not seen in naïve or sham rats.

Intra-ACC Drug Application

Three days after CCI or sham surgery, rats were anesthetized with 4% chloral hydrate (10 ml/kg, intraperitoneal) and placed into a digital stereotaxic device (Narishige, Japan) with bregma and lambda at the same horizontal level. A glass pipette (10- to 15-μm diameter tip) connected to a 10-μl Hamilton syringe driven by an automated syringe pump (Stoelting Co., USA) was inserted into the right ACC (from bregma: anteroposterior, 2.2 mm; mediolateral, 0.7 mm; dorsoventral, 2.4 mm for adult rats; anteroposterior, 1.2 mm; mediolateral, 0.35 mm; dorsoventral, 1.75 mm for young rats) or into the left pontine nuclei and surrounding pyramidal tracts (from bregma: anteroposterior, −7.0 mm; mediolateral, −2.0 mm; dorsoventral, 9.4 mm for adult rats) according to the rat brain atlas.[24] A volume of 0.5 μl of cholera toxin subunit B (CT-B; Alexa Fluor 488, dissolved in 0.01 M phosphate buffered saline [PBS], 1 μg/μl; ThermoFisher Scientific, USA) was injected over a 5-min period. The injection pipette was left in place for an additional 5 min to minimize the efflux of the drug or cerebrospinal fluid. Rats were allowed to recover for at least 4 days before their use in other experiments.

For drug application in behavioral experiments, a 30-gauge stainless steel guide cannula with a 33-gauge stainless steel stylet plug (Shenzhen RWD Life Science Co., Ltd., China) was bilaterally inserted in adult rats, 0.5 mm above the ACC injection site. The rats were given 1 week to recover from the cannula implantation. Microinjections were performed on awake rats through a 33-gauge stainless steel injection cannula linked to a syringe pump (Stoelting Co.) by a long flexible pipe. The injection cannula was extended 0.5 mm beyond the tip of the guide cannula and a volume of 0.5 μl per hemisphere of 6×10^8 transducing units of short hairpin RNA (shRNA), negative control shRNA (shNC), 9-(dimethylamino)-3-(hexahydro-1*H*-azepin-1-yl)pyrido[3′,2′:4,5]thieno[3,2-*d*]pyrimidin-4(3*H*)-one (A841720; 2 μg/μl), or artificial cerebrospinal fluid (aCSF;

6% dimethyl sulfoxide [DMSO]) was injected. Rats were allowed to recover for 30 min before the first behavioral test.

Immunofluorescence

At designated time points, rats were anesthetized with 4% chloral hydrate (10 ml/kg, intraperitoneal) and perfused through the ascending aorta with 300 ml of 0.9% saline, followed by 300 ml of 4°C 4% paraformaldehyde (in 0.1 M sodium phosphate buffer, pH 7.4). Brains were quickly removed and postfixed for 24 h in phosphate-buffered 4% paraformaldehyde at 4°C. After dehydration in 30% phosphate-buffered sucrose solution for at least 3 days, the frozen brains containing ACC (bregma, 2.70 to 1.70 mm) were coronal sectioned into slices at 25 μm in thickness with a cryostat (1900, Leica, Germany). The injection sites and transfection range of CT-B and lentivirus were confirmed by consecutive brain sections showing the green fluorescence. The depths of the upper and lower laminar boundaries of L5 were defined as 40.6% and 69.5% of overall cortical thickness of the ACC, respectively.[25]

For hyperpolarization-activated/cyclic nucleotide-gated (HCN) channel subtype 1/CT-B, Kv2.1/CT-B, or Kv2.2/CT-B double-labeled immunofluorescence, the slices were incubated with 10% normal goat serum in 0.01 M PBS for 30 min at 37°C and then incubated with a mouse monoclonal HCN1 antibody (1:200; Abcam, United Kingdom), a mouse monoclonal Kv2.1 antibody (1:400; Abcam), or a mouse monoclonal Kv2.2 antibody (1:400; Abcam) overnight at 4°C. After three rounds of 10-min rinses in PBS, the sections were incubated in Cy3-conjugated goat antimouse immunoglobulin G (1:200; Invitrogen, USA) for 1 h at 37°C and then counterstained with 4′,6-diamidino-2-phenylindole (Sigma-Aldrich, USA) for 10 min at 37°C and washed in PBS. Each slice was coverslipped with a mixture of 50% glycerin in PBS and then observed with a confocal laser scanning microscope (Leica DMI 6000, Wetzlar, Germany). The specificities of the immunostaining and primary antibodies were verified by omitting the primary antibodies or conducting the preabsorption experiments,[26] respectively. Five slices were extracted from a total of 21 consecutive slices containing CT-B (four slices per interval) of each brain for statistical analysis.

Brain Slices Preparation

The male Sprague–Dawley rats (P28 to P31), 7 days after CCI or sham surgery, were rapidly decapitated, and the brain was quickly removed and submerged in a 0°C, preoxygenated (95% O_2, 5% CO_2) sucrose solution containing the following (in mM): 220 sucrose, 10 D-glucose, 1.25 Na_2HPO_4, 26 $NaHCO_3$, 2.5 KCl, 6 $MgCl_2$, and 1 $CaCl_2$. Coronal slices (300 μm), including the ACC (1.6 to 0.7 mm rostral to the bregma), were prepared using an oscillating tissue slicer (VT1000, Leica) and transferred to an incubation chamber filled with aCSF, containing the following (in mM): 119 NaCl, 2.5 KCl, 2.5 $CaCl_2$, 1.3 $MgCl_2 \cdot 6\ H_2O$, 1.25 $NaH_2PO_4 \cdot 2\ H_2O$, 26.2 $NaHCO_3$, and 11 D-glucose, and aerated with a mixture of 95% O_2–5% CO_2 at 31° to 33°C before recording. After incubation for a minimum of 90 min, slices were transferred to a submersion-type recording chamber and perfused with constantly aerated aCSF at a rate of 1 to 2 ml/min.

Whole Cell Clamp Recordings and Data Analysis

Whole cell recordings in rat brain slice neurons were performed as described previously,[7] and the recordings were blinded to the slice preparation. ACC L5 PNs (0.6 to 0.8 mm below the pial surface, contralateral to the CCI surgery) were targeted for recording using an upright microscope equipped with Leica infrared-differential interference contrast optics, a 340 water-immersion objective, and a charge coupled device camera. The CT-B–labeled neurons were visualized using a mercury lamp with a filter set. Recording electrodes made from 1.5-mm glass capillaries were pulled on a Flaming–Brown micropipette puller (P-97, Shutter Instrument, USA) and filled with internal solution containing the following (in mM): 145 potassium gluconate, 5 HEPES, 0.5 EGTA, 2 $MgCl_2$, and 5 K_2ATP (pH 7.2 to 7.4). With this solution, the recording electrode exhibited a resistance of 2.5 to 6.0 MΩ. Liquid junction potentials were corrected arithmetically at the beginning of the experiment. Recordings were performed at 31° to 33°C. After gigaohm seal formation and patch rupture, series resistance was compensated 60 to 80% and continually monitored throughout the experiment. In voltage clamp experiments, capacitative transients were reduced by the electronic capacitance compensation in the amplifier circuit. The current clamp recordings were performed in bridge mode to allow for faithful voltage after.[27] Neurons were given at least 5 min to stabilize before data collection and were discarded if the series resistance increased by more than 20%. The signals were lowpass filtered at 5 kHz using a MultiClamp 700B amplifier (Molecular Devices, USA), digitized at 10 kHz with a digitizer (Digidata 1440A, Molecular Devices), and stored for offline analysis with pClamp9.2 software (Molecular Devices). The external solution was standard aCSF for current-clamp experiments and aCSF with 500 nM tetrodotoxin for voltage-clamp experiments.[28]

Data were analyzed using Clampfit (Molecular Devices), MATLAB (Mathworks, USA), and Microsoft Excel (Microsoft Corporation, USA). Thirteen neurons from a total of 184 recording neurons were discarded because the series resistance increased by more than 20%. Beyond that, no data were excluded from the statistical analysis. The resting membrane potential (RMP) was measured immediately after breaking into the cell. Input resistance was calculated from the linear portion of the current–voltage relationship generated in response to a series of 1000-ms current injections (–300 to +50 pA, 50-pA steps). The voltage sag ratio was determined by the function $[100 \times (V_{ss} - V_{min})/(V_{bsl} - V_{min})]$, where V_{ss} is steady-state voltage, V_{min} is minimum voltage, and V_{bsl} is baseline voltage, at a negative current step that caused an approximately –20-mV

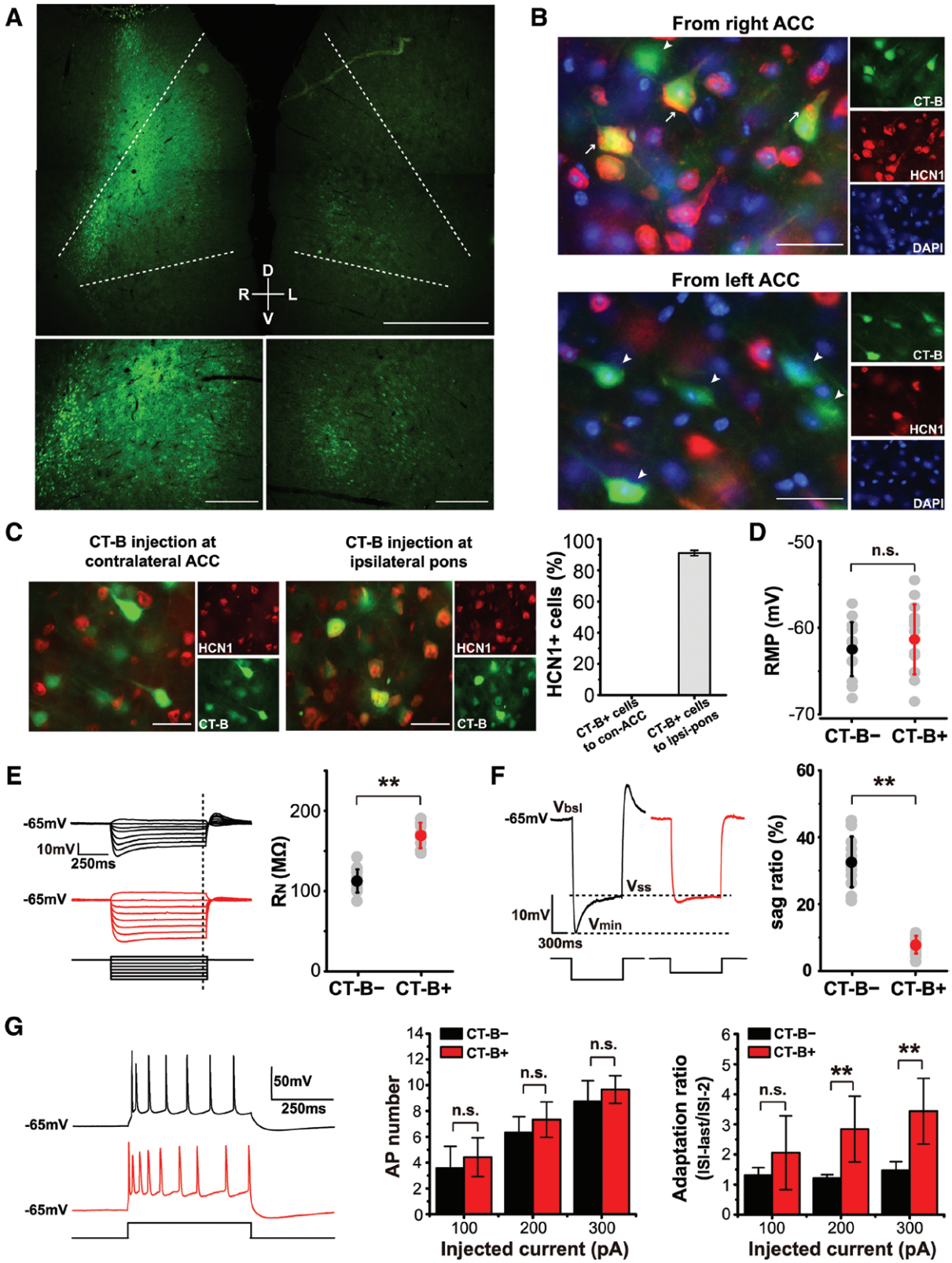

Fig. 1. Electrophysiology of anterior cingulate cortex (ACC) layer 5 pyramidal neurons (L5 PNs) depends on the long-range projection targets. (*A*, *top*) Retrograde labeling of the left ACC L5 PNs after injection of Alexa Fluor 488–labeled cholera toxin subunit B (CT-B) into the right ACC. The *white dashed lines* represent the location of ACC. *Scale bar* = 1000 μm. D = dorsal; L = left; R = right; V= ventral. (*A*, *bottom*) Magnified images showing the CT-B positive (CT-B+) neurons in the right and left ACC. *Scale bar* = 200 μm. (*B*) Magnified images showing CT-B and hyperpolarization-activated/cyclic nucleotide-gated (HCN) channel subtype 1

(*Continued*)

Fig. 1. (*Continued*) double labeling in the right (*top*) and left (*bottom*) ACC. The CT-B is injected into the right ACC. *Scale bar* = 50 μm. *Arrows* indicate the colocalizations of CT-B and HCN1. *Arrowheads* indicate the CT-B+ neurons that do not show HCN1 immunoreactivity. (*C*, *left*) Magnified images showing CT-B and HCN1 double labeling in the left ACC after injection of CT-B into the right ACC or the left pons and surrounding pyramidal tracts. *Scale bar* = 50 μm. (*C*, *right*) Percentages of HCN1+ cells in CT-B+ cells that project to contralateral ACC (con-ACC, n = 6 rats) or ipsilateral-pons (ipsi-pons, n = 3 rats). (*D*) Resting membrane potentials of CT-B negative (CT-B–) and CT-B+ ACC L5 PNs are comparable. Unpaired Student's *t* test, all groups n = 14. For this and the following figures in this format, the *gray dots* represent data from individual cells, and the *black/red dots* and *bars* represent mean ± SD. (*E*, *left*) Representative traces showing the voltage responses to a series of current stimuli (–300 to +50 pA, step = 50 pA). *Dashed line* represents that the input resistance was measured at the end of 1000-ms current steps. (*E*, *right*) CT-B+ ACC L5 PNs have significantly larger steady-state input resistance than CT-B– neurons. Unpaired Student's *t* test, all groups n = 14. (*F*, *left*) Representative traces of voltage sag induced by a current step that caused an approximately –20 mV hyperpolarization at steady state. V_{bsl} = baseline voltage; V_{min} = minimum voltage; V_{ss} = steady-state voltage. (*F*, *right*) CT-B+ ACC L5 PNs have a prominently smaller sag ratio than CT-B– neurons. Unpaired Student's *t* test, all groups n = 12. (*G*, *left*) Representative traces showing the firing response to a depolarizing current stimulus (+300 pA, 500 ms). (*G*, *middle*) The number of action potentials (APs) elicited by depolarizing current steps of varying amplitude are not significantly different between CT-B– and CT-B+ neurons. Unpaired Student's *t* test, all groups n = 12. (*G*, *right*) CT-B+ ACC L5 PNs have a larger adapting ratio than CT-B– neurons, especially during +200 pA and +300 pA current stimuli. Unpaired Student's *t* test, all groups: CT-B– n = 8, CT-B+ n = 12. ISI = interspike interval; n.s. = no significant difference, $^{*}P < 0.05$, $^{**}P < 0.01$.

hyperpolarization of the membrane potential (fig. 1). In this way, differences in input resistance were compensated.[8] Single APs were analyzed for AP threshold, AP peak, maximum derivative of the voltage with respect to time (dV/dt), AP half-width, and AP width. The AP threshold was calculated as the point where the first derivative of the upsweep of the spike equaled 10 V/s. The AP half-width and AP width measurements were taken at half the AP peak amplitude relative to the threshold or at the AP threshold, respectively. The fAHP potential measurement was obtained when the mean first derivative of the trace reached 0.0 ± 0.5 V/s after each spike, using a 1-ms sliding average.[29] The AHP was defined as the difference in the membrane potential 50 ms before the onset of the stimulus and the minimum voltage after the spike train.

Western Blot

Western blot experiments were performed as described previously.[7] In brief, rats were euthanized at designated time points. The ACC was quickly dissected on ice using a rat brain matrix (Stoelting Co.), and protein was extracted by T-PER tissue protein extraction reagent (Pierce, USA). Equal amounts of protein (50 μg) were loaded and separated in 8% Tris-Tricine sodium dodecyl sulfate polyacrylamide gel electrophoresis. The resolved proteins with desired molecular weight were transferred onto polyvinylidene fluoride membranes (GE Healthcare Bio-Science, USA). Then the membranes were blocked in 5% nonfat milk (containing Tris-buffered saline, 0.1% Tween-20, pH 7.4) for 2 h at 37°C and then incubated overnight at 4°C with mouse monoclonal Kv2.2 antibody (1:400; Abcam) or rabbit β-actin antibody (1:1000; Zhongshan Goldenbridge Biotechnology, China). The blots were washed three times in Tris-buffered saline, 0.1% Tween-20 for 10 min and then incubated with the secondary antibody, goat anti-mouse or anti-rabbit immunoglobulin G conjugated with horseradish peroxidase (1:1000; Zhongshan Goldenbridge Biotechnology) for 1 h at 37°C. Finally, signals were visualized using enhanced chemiluminescence (Pierce ECL, ThermoFisher Scientific) and exposed with the ChemiDoc XRS system (Bio-Rad Laboratories, USA).

The density of specific bands was measured using the Quantity One software (Bio-Rad Laboratories) for quantification. The same size square was drawn around each band to measure the density, and the background near that band was subtracted. β-Actin was used as the internal control. Kv2.2 level was normalized against β-actin level and expressed as a fold increase compared with sham group.

Behavioral Measurements

The tests of thermal and mechanical threshold were conducted on the ipsilateral hind paws of sham and CCI rats, as described previously,[21] and the experiments were blinded to drug application. All of the rats were pre-exposed to the experimental chamber for 3 h per day for 3 days before the behavioral tests for habituation. Thermal hyperalgesia was assessed using the test by Hargreaves *et al.*[30] Rats were individually placed in Plexiglas chambers on a glass platform, under which a radiant heat source (IITC Life Science, USA) was directed at the proximal half of the hind paw plantar surface. The heat source was turned off immediately when the rat briskly lifted the foot, allowing the measurement of the paw withdrawal thermal latency as the threshold of thermal sensitivity. Each hind paw was tested five times at 2-min intervals, and a 60-s cutoff was used to prevent tissue damage in the absence of a response.

Mechanical allodynia measurements were carried out using a calibrated series of von Frey hairs with bending forces at a range of 0.3 to 60.3 g. Tests were initiated with 4.10 g of von Frey hairs, the middle of the filament series. The filament was applied to the plantar surface of the hind paw with a sufficient force to bend it for 2 s. A positive paw withdrawal response was recorded if the hind paw was briskly lifted and completely removed from the platform. The 50% paw-withdrawal mechanical threshold was determined by the up-down method.[31]

Drugs

All of the reagents were obtained from Sigma-Aldrich with the exception of guangxitoxin-1E (GxTX), (*RS*)-3,5-dihydroxyphenylglycine (DHPG), phorbol 12-myristate 13-acetate (PMA), and A841720 from Tocris Bioscience (United Kingdom), as well as CT-B (Alexa Fluor 488) from ThermoFisher Scientific/Molecular Probes. During whole cell recording, all of the drugs were dissolved in their suitable solvents as stock solutions and were applied by switching the perfusion from aCSF to a solution containing the desired drug at an appropriate concentration. Bath-applied drugs were perfused for at least 5 min to ensure complete equilibration within the recording chamber. For intra-ACC application, A841720 was dissolved in DMSO as stock solution and diluted by aCSF to the desired concentration before microinjection. The vehicle solution was an aCSF containing 6% DMSO, consistent with the final concentration of DMSO in A841720 working solution. All of the stock solutions were stored in tightly sealed vials at −20°C and used within 1 month.

shRNA targeting the rat *Kv2.2* gene (Kcnb2; GenBank accession No. NM_054000) and nontargeting shNC sequences were designed and synthesized by Shanghai GeneChem Co., Ltd. (China). The sequence of Kv2.2-shRNA and shNC were 5′-AAGGAGCAGATGAACGAAGAA-3′ and 5′-TTCTCCGAACGTGTCACGT-3′, respectively. The recombinant virus expressing enhanced green fluorescent protein was packaged using a Lentivector Expression Systems kit (Shanghai GeneChem Co., Ltd).

Statistical Analysis

No statistical analyses were used to predetermine the sample size, but our sample sizes were based on previous reports[32,33] and our previous publication.[7] All of the quantitative values were normally distributed and expressed as the mean ± SD. Statistical comparisons were made using SPSS version 19 software (SPSS Inc., USA). All of the comparisons between the two groups were analyzed using Student's unpaired *t* test. One-way ANOVA, followed by *post hoc* Bonferroni multiple comparison tests, was used to compare the AP numbers and the relative protein level. The comparison of cumulative probability distribution of interspike interval (ISI) was analyzed using the Kolmogorov–Smimov test. For the current threshold of entry into depolarization block, Kruskal–Wallis test followed by Dunn-Bonferroni *post hoc* test was used because equal variance was not assumed. The instantaneous frequency, fAHP, AP width, all of the current densities evoked by a series of voltage steps, and all of the thermal and mechanical thresholds were analyzed using two-way repeated-measures ANOVA followed by *post hoc* Bonferroni multiple comparison tests. The comparison of current density (evoked by 30-mV depolarization) predrug and postdrug application was made using one-way repeated-measures ANOVA followed by *post hoc* Bonferroni multiple comparison tests. In all of the cases, $P < 0.05$ (two-tailed test) was considered to be statistically significant. Lastly, "n" referred to the number of recording cells unless stated otherwise.

Results

Contralateral-projecting ACC L5 PNs Have Unique Intrinsic Properties

To confirm that ACC L5 PNs exhibited heterogeneity based on their long-range projection targets, we infused the retrograde tracer, CT-B (Alexa Fluor 488,),[34] into the right ACC (fig. 1A).[9] Thus, the commissural ACC L5 PNs projecting to the contralateral ACC were labeled by CT-B in the left ACC (fig. 1A), whereas the corticopontine L5 PN was CT-B absent. Given that the corticopontine neurons in mPFC have distinct electrophysiologic properties, particularly in the sag ratio, which reflects the activation of HCN ion channels, relative to the commissural neurons,[9] we performed double-labeled immunofluorescence to examine whether the expression of HCN channels in ACC L5 was also different between these two cell subtypes. In the right ACC, that is, the CT-B infusion site, we observed robust HCN1 (the predominantly expressed HCN channel subtype in the prefrontal cortex) immunoreactivity on the membrane and apical dendrite of CT-B-positive (CT-B+) L5 PNs (fig. 1B, top), and there were also many CT-B+ neurons exhibiting no HCN1 immunoreactivity. However, in the left ACC, we did not find any CT-B+ L5 PNs showing HCN1 immunoreactivity under the same imaging settings (fig. 1B, bottom). These results suggest that HCN1 is mainly expressed on corticopontine neurons in ACC L5, whereas the commissural neurons expressed little, if any HCN1. In the right ACC, both neuronal types were infected by CT-B because the infection was nonselective. However, in the left ACC, only the commissural neurons projecting to the contralateral infusion site were CT-B+. To further confirm this hypothesis, we injected CT-B into either the left pontine nuclei or right ACC to separately label the corticopontine or commissural neurons in the left ACC (fig. 1C). We observed that, under the same imaging settings, nearly 91% of the corticopontine neurons were labeled by HCN1, but none of the commissural neurons were HCN1 positive.

Thus, we injected CT-B into the right ACC of young rats to mark the commissural neurons in the left ACC, and we also named these neurons CT-B+ neurons in the following experiments. Next, we examined whether the CT-B+ and CT-B-negative (CT-B–) L5 PNs in the left ACC had distinct electrophysiologic properties. The RMPs of the two subtypes were identical (fig. 1D). To perform more accurate comparisons, we adjusted the holding current such that the membrane potential was −65 mV. CT-B– neurons had a significantly smaller steady-state input resistance (R_N) compared with CT-B+ neurons (fig. 1E). Consistent with the difference in R_N, we found that CT-B– neurons had a prominently larger voltage sag ratio than CT-B+ neurons in a nonoverlapping manner (fig. 1F), similar to a previous

Table 1. Passive Membrane Properties of CT-B+ ACC L5 PNs Are Not Changed after CCI

Variable	Naïve (n = 14)	Sham (n = 14)	CCI (n = 14)	$F_{(2,39)}$	*P* Value
RMP (mV)	−61.34 ± 4.02	−61.25 ± 4.09	−61.87 ± 3.20	0.109	0.897
Cm (pF)	90.00 ± 52.33	96.01 ± 38.56	97.75 ± 37.51	0.123	0.884
R_N (MΩ)	169.29 ± 15.73	164.37 ± 41.89	163.38 ± 33.23	0.135	0.874
Rheobase (pA)	52.14 ± 11.22	59.29 ± 12.69	57.86 ± 8.93	1.637	0.208

Comparison of resting membrane potential (RMP), membrane capacitance (Cm), input resistance (R_N), and rheobase of cholera toxin subunit B (CT-B)+ anterior cingulate cortex (ACC) layer 5 pyramidal neurons (L5 PNs) among naïve, sham, and chronic constriction injury (CCI) rats. Data were calculated with one-way ANOVA.

report in mPFC.[35] Then we injected a series of depolarizing currents (100 to 300 pA, step = 100 pA) for 500 ms to test the firing properties of the two subtypes (fig. 1G). Although both neuronal types fired at nearly the same rate, the CT-B+ neurons displayed a much higher spike frequency adaptation ratio, particularly during 200 and 300 pA stimuli, compared with the CT-B– neurons. These results indicated that the L5 PNs in ACC, similar to the mPFC, could be divided into at least two subtypes.

Altered Cellular Excitability of CT-B+ ACC L5 PNs in CCI Rats

The modifications of CT-B– ACC L5 PNs contralateral to the sciatic nerve lesion, which expressed many HCN1 channels, have been relatively well studied in the CCI condition.[6] Thus, we aimed to explore the potential changes of CT-B+ neurons using the successfully established CCI model.[7] We first evaluated the passive membrane properties of the CT-B+ ACC L5 PNs from naïve, sham, and CCI rats on day 7 after CCI. There were no significant differences in the RMP, membrane capacitance, R_N and rheobase of the CT-B+ neurons among naïve, sham, and CCI groups (table 1). Next, we investigated the neuronal excitability by characterizing the AP firing patterns. When the membrane potential was held at −65 mV and an identical rheobase current was injected for 10 s (fig. 2A), the CT-B+ neurons in CCI slices displayed a significantly higher AP firing rate than the neurons from naïve slices (fig. 2B). Although the AP numbers of sham and CCI neurons were not significantly different, the cumulative probability distribution of the ISI of the CCI neurons was obviously leftward shifted compared with sham neurons (fig. 2C), which also reflected an increase in firing frequency. Then we elicited AP firing by

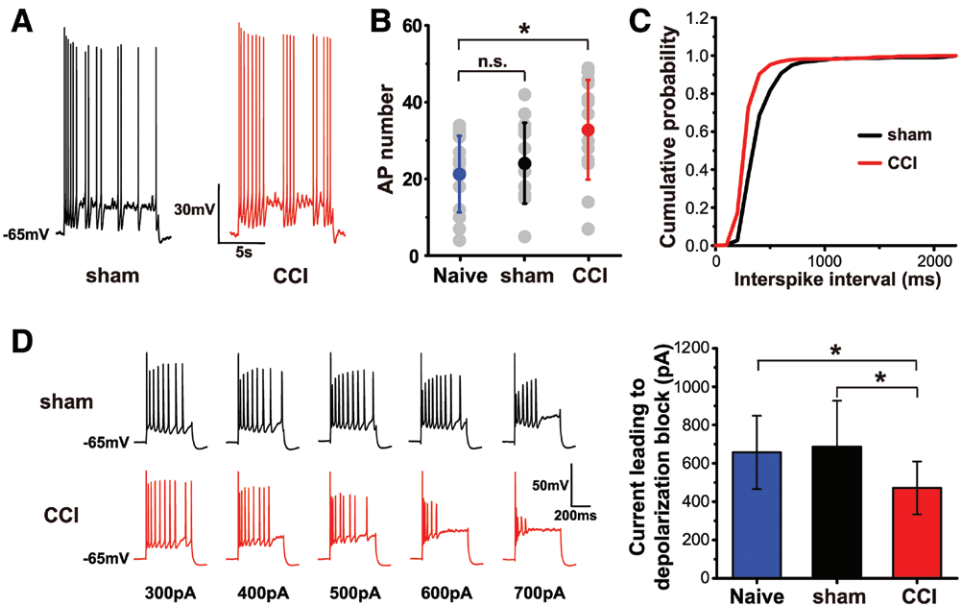

Fig. 2. The tonic firing frequency of cholera toxin subunit B (CT-B)+ anterior cingulate cortex (ACC) layer 5 pyramidal neurons (L5 PNs) is increased after chronic constriction injury (CCI). (*A*) Representative traces showing the firing response of CT-B+ neurons to a 10-s rheobase stimulus. (*B*) The firing number elicited by the rheobase stimulus increases significantly in the CCI group compared with the naïve group. One-way ANOVA and *post hoc* Bonferroni multiple comparison tests, all groups n = 14. (*C*) CCI surgery induces an obvious leftward shift of the interspike interval cumulative distribution curve. Kolmogorov–Smimov test, $P < 0.01$. (*D*, *left*) Representative traces showing the firing response to a series of depolarizing current stimulus (+300 to +700 pA, 500 ms). (*D*, *right*) The current threshold of entry into the depolarization block of CCI CT-B+ neurons is significantly lower than that of the other two groups. Kruskal–Wallis test and Dunn-Bonferroni *post hoc* test, all groups n = 14. n.s. = no significant difference, $^*P < 0.05$, $^{**}P < 0.01$.

applying depolarizing currents (100 to 1000 pA, step = 100 pA) in 500-ms duration to fully analyze the spiking responses to the suprathreshold stimuli. However, considerable amounts of recording neurons (8 of 42) started to enter the depolarization block from the 400-pA stimulation, and during the 1000-pA stimulation, a majority (36 of 42) of recording neurons exhibited depolarization block. Moreover, the CT-B+ neurons in the CCI group notably showed an increased propensity to enter the depolarization block compared with neurons from other two groups (fig. 2D).

Thus, we focused on the APs elicited by the weaker and perhaps physiologically more pertinent stimuli (100, 200, and 300 pA; fig. 3A) and observed that the mean AP number fired by each of these stimuli in CT-B+ neurons from the CCI group was much more than those from the other two groups (fig. 3B). Hence, we used the 300-pA stimulus as an example and compared the spike frequency adaptation ability of the CT-B+ neurons from different groups by measuring the first 7 ISIs. All of the groups exhibited an initial period of high-frequency AP generation followed by an accommodation to a much lower steady-state firing frequency, but the CCI neurons fired obviously at a higher frequency (fig. 3C). Furthermore, we observed a significantly higher instantaneous firing frequency at steady-state in CCI neurons, whereas the firing frequency at onset was not significantly different between groups (one-way ANOVA: frequency at onset: $F_{(2,21)} = 1.354$, $P = 0.280$; steady-state frequency: $F_{(2,21)} = 12.724$, $P = 0.000$; fig. 3C).

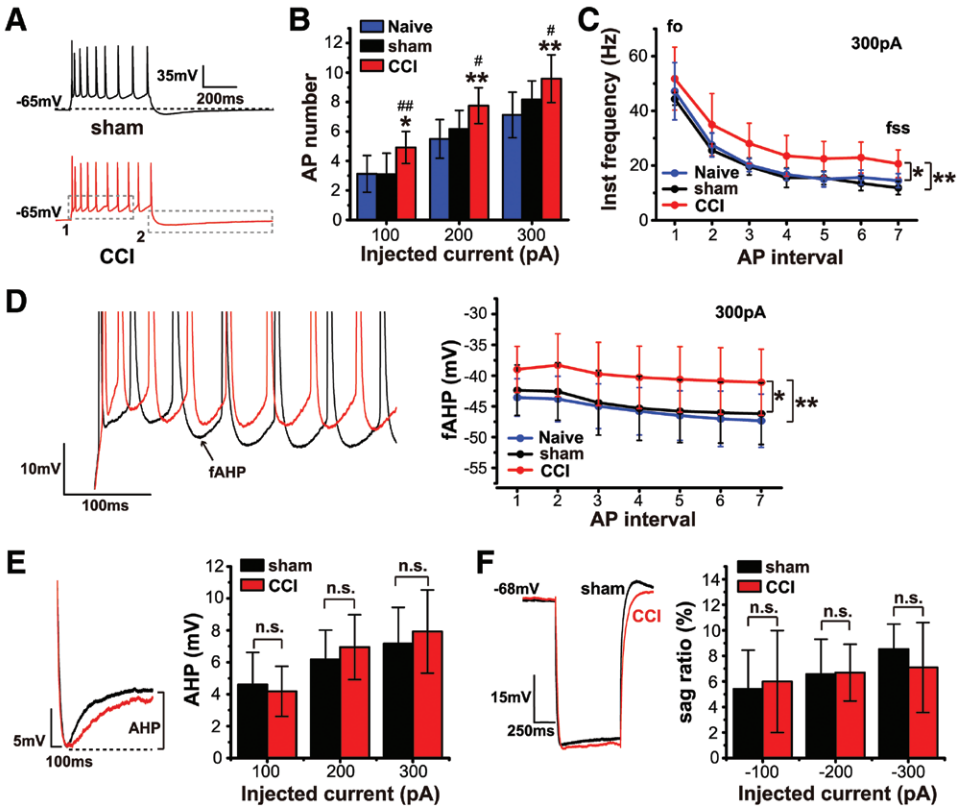

Fig. 3. Firing properties of cholera toxin subunit B (CT-B)+ anterior cingulate cortex (ACC) layer 5 pyramidal neurons (L5 PNs) are changed after chronic constriction injury (CCI). (*A*) Representative traces showing the firing response to a depolarizing current stimulus (+300 pA, 500 ms). *Black dashed line* represents that the membrane potential finally returned to the level of beginning. (*B*) The action potential (AP) number of CT-B+ neurons increases significantly after CCI in each depolarizing current step. One-way ANOVA and *post hoc* Bonferroni multiple comparison tests, all groups: CCI and sham n = 12, naïve n = 8; *,** *versus* naïve, $^{\#,\#\#}$ *versus* sham. (*C*) The comparison of instantaneous frequency of AP firing in response to a 300-pA current injection, data are presented for the first seven spike intervals (*i.e.,* eight spikes). CCI neurons fire APs at a significantly higher frequency. Two-way repeated-measures ANOVA and *post hoc* Bonferroni multiple comparison tests, all groups n = 8; fo = onset frequency; fss = steady-state frequency. (*D*, *left*) Expanded view of merged traces in the *gray rectangle* (*1*) in *A*. (*D*, *right*) CCI neurons show a much higher fast afterhyperpolarization potential during each AP interval. Two-way repeated measures ANOVA and *post hoc* Bonferroni multiple comparison tests, all groups n = 12. (*E*, *left*) Expanded view of merged traces in the *gray rectangle* (*2*) in *A*. (*E*, *right*) The postburst afterhyperpolarization potentials elicited by depolarizing current steps of varying amplitude are not significantly different between sham and CCI CT-B+ neurons. Unpaired Student's *t* test, all groups n = 12. (*F*, *left*) The comparison of voltage sag at –300 pA. (*F*, *right*) The voltage sags elicited by hyperpolarizing current steps of varying amplitude are identical between sham and CCI CT-B+ neurons. Unpaired Student's *t* test, all groups n = 6. n.s. = no significant difference, $^{*}P < 0.05$, $^{**}P < 0.01$, $^{\#}P < 0.05$, $^{\#\#}P < 0.01$.

AP Shape of CT-B+ ACC L5 PNs Was Changed after CCI

Next, we aimed to explore the potential mechanisms underlying hyperexcitability. It had been shown that the fAHP plays an important role in determining the spike frequency during burst firing. Thus, we assessed the first 7 fAHPs during the 300-pA stimulus and found that the CT-B+ ACC L5 PNs in the CCI group exhibited substantially higher fAHP potentials compared with neurons in the naïve and sham groups (fig. 3D). Given that the postburst slow AHP reflecting a Ca^{2+}-activated K^+ conductance also played a critical role in shaping the pattern of AP generation,[36,37] we compared the slow AHP of sham and CCI CT-B+ neurons. However, there was no significant difference between the two groups in each of the depolarizing stimuli (fig. 3E). In addition, we also revealed by measuring the sag ratios that the tiny I_h of the sham and CCI CT-B+ neurons were comparable (fig. 3F).

Moreover, we compared the AP waveforms in the sham and CCI CT-B+ neurons because the changes of AP repolarization would lead to an alteration in fAHP. In all of the neurons, the AP waveforms were dynamic and exhibited progressively smaller spikes.[27] For this reason, we concentrated our analysis on the properties of the first and seventh APs triggered by a 300-pA depolarizing stimulus to compare the APs at the onset or steady state of a 500-ms burst. Figure 4, A and B plotted the example waveforms of such APs and their corresponding phase plots. There was no difference in AP threshold, peak potential, or maximum dV/dt between groups (fig. 4C). However, we observed a significant difference in the half-width of seventh APs between the sham and CCI CT-B+ neurons (fig. 4D). The precise measurements of the first seven AP widths to capture the changes on the late phase of repolarization[28] further revealed a larger and obvious increase after CCI (fig. 4E).

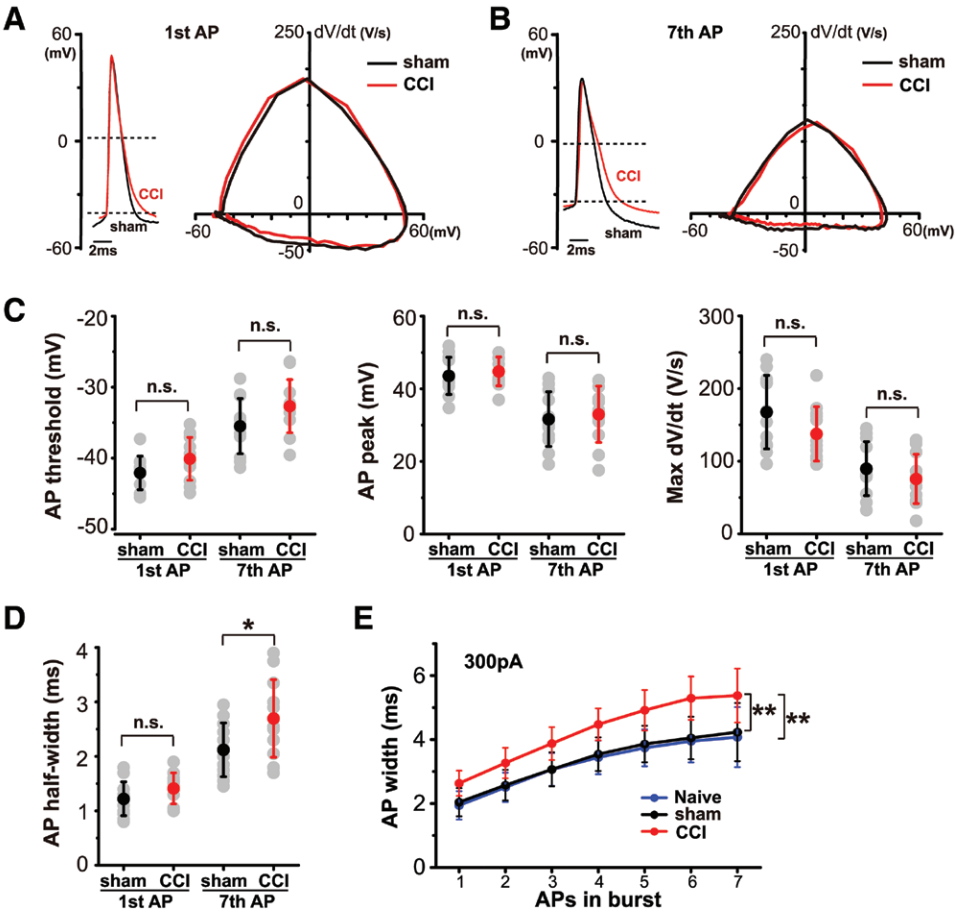

Fig. 4. Action potential waveforms of cholera toxin subunit B (CT-B)+ anterior cingulate cortex (ACC) layer 5 pyramidal neurons (L5 PNs) are altered after chronic constriction injury (CCI). (*A*) The comparison of action potential (AP) waveforms and their corresponding phase plots of the first APs elicited by a 300-pA depolarizing stimulus. (*B*) The comparison of AP waveforms and their corresponding phase plots of the seventh APs elicited by a 300-pA depolarizing stimulus. (C) The first or seventh AP threshold (*left*), peak potential (*middle*), and maximum rate of rise (*right*) are not significantly different between sham and CCI CT-B+ neurons. Unpaired Student's *t* test, all groups n = 12. (*D*) The half-widths of first APs are unchanged whereas the half-widths of seventh APs are obviously increased after CCI. Unpaired Student's *t* test, all groups n = 12. (*E*) The comparison of AP width of firing in response to a 300-pA current injection, data are presented for the first seven spikes. CCI neurons have much broader AP widths. Two-way repeated-measures ANOVA and *post hoc* Bonferroni multiple comparison tests, all groups n = 12. dV/dt = derivative of the voltage with respect to time; max = maximum; n.s. = no significant difference. *P < 0.05, **P < 0.01.

Kv2 Currents of CT-B+ ACC L5 PNs Were Inhibited after CCI

Our data described above indicated a decrease in the rate of spike repolarization (specifically in the late phase, resulting in an increase in AP width) in CT-B+ ACC L5 PNs after CCI, accompanied by an increase of fAHP potentials. Among the numerous channels contributing to AP kinetics, the voltage-gated potassium channels mainly contribute to AP repolarization. Particularly, the Kv2 channels producing the bulk of delayed-rectifier currents are broadly expressed across the mammalian brain[38–40] and are mainly responsible for the late falling phase and fAHP of the APs within bursts,[28] making them the key regulators of neuronal excitability.[41–43] In addition, previous reports have also suggested that inhibition of A-type K^+ currents (I_A) result in an increase in the AP width and decrease in the fAHP.[29] Therefore, we investigated depolarization-activated potassium currents in CT-B+ ACC L5 PNs using selective blockers.

Figure 5A shows the composition of the total depolarization-activated potassium currents in these neurons from the sham group, evoked by a voltage step from −90 to 60 mV. Application of 100 nM GxTX[41] nearly completely inhibited the Kv2-mediated current during the entire depolarizing step, particularly in the steady-state phase. Additional application of 2 mM 4-aminopyridine (4-AP)[29] prominently inhibited the peak current corresponding with I_A but did not influence the steady-state current in which I_A had inactivated. The remaining current after application of GxTX and 4-AP might contain the BK calcium-activated potassium current and other depolarization-activated currents.

Then we compared the total depolarization-activated potassium currents between the CT-B+ ACC L5 PNs from the sham and CCI groups. We observed that the CT-B+ neurons from the CCI group showed significantly smaller total outward currents measured at both the peak and steady state (fig. 5B). However, after application of 100 nM GxTX, this difference was absent (fig. 5C). The comparison of GxTX-sensitive currents at steady state by subtracting the currents after GxTX application from the total outward currents revealed a significant difference (fig. 5D). We further applied 4-AP during bath application of GxTX and found that neither the residual current (fig. 5E) nor the 4-AP–sensitive current (fig. 5F) was different between the sham and CCI groups. These results suggested that the Kv2-mediated, GxTX-sensitive currents in CT-B+ neurons were obviously inhibited after CCI.

Inhibition of mGluR1 Rescued the Decreased Kv2 Current in CT-B+ ACC L5 PNs after CCI

A previous study demonstrated that CCI induced an increase in ACC extracellular glutamate concentration,[26] which might have led to an overactivation of both ionotropic and metabotropic glutamate receptors on the postsynaptic membrane. Moreover, inhibition of mGluR1 has been shown to modulate the excitability of HCN1-positive ACC L5 PNs after CCI,[7] producing an analgesic effect. Thus, we tested the hypothesis that inhibition of mGluR1 could attenuate the reduction of Kv2 current in CT-B+ neurons. We used the voltage step from −60 to 30 mV to evoke the total outward current, because the I_A was unaltered after CCI and was nearly completely eliminated by the holding potential of −60 mV. Moreover, the 30-mV depolarization was physiologically more pertinent.

We first examined whether mGluR1 activation could down-regulate the Kv2 current of CT-B+ ACC L5 PNs in sham rats. Bath application of 5 min of DHPG (15 μM), an agonist of group 1 mGluRs, dramatically decreased the total outward current in sham slices (fig. 6A). After a 20-min rinse, the total outward current recovered to predrug level. However, in the presence of 100 nM GxTX, which nearly entirely abolished the Kv2 current (fig. 6B), DHPG exerted no additional effect (Bonferroni multiple comparison tests: P = 0.927, GxTX *vs.* GxTX+DHPG; fig. 6B), suggesting that DHPG inhibited the Kv2 current to reduce the total outward current. Blockade of mGluR1 in sham slices by 10 μM A841720 (mGluR1 antagonist) had no effect on the total outward current (fig. 6C). However, in the presence of A841720, the application of DHPG failed to reduce Kv2 current (Bonferroni multiple comparison tests: P = 1.000, A841720 *vs.* A841720+DHPG; fig. 6C), further suggesting that the effect of DHPG was mGluR1 mediated.

Next, we tested whether blockade of mGluR1 in CCI rats could rescue the Kv2 current of CT-B+ ACC L5 PNs. As shown in figure 6D, application of 10 μM A841720 produced a marked increase in the total outward current. Consistent with the expectation, the effect of A841720 was Kv2 mediated because preapplication of 100 nM GxTX prevented this effect (Bonferroni multiple comparison tests: P = 1.000, GxTX *vs.* GxTX+A841720; fig. 6E). In addition, we observed that 15 μM DHPG could additionally reduce the total outward current in CCI CT-B+ neurons (fig. 6F) to a level identical with its effect in sham slices (sham + DHPG: fig. 6A, CCI + DHPG: fig. 6F; Unpaired Student's t test: P = 0.398). Considering that the Kv2 current before DHPG incubation was significantly smaller in CCI CT-B+ neurons than in the sham group, the effect of DHPG in CCI slices might be weaker, indicating that the mGluR1 had been prominently activated after CCI.

Protein Kinase C Mediated the Regulatory Effect of mGluR1 on Kv2 Current

The mGluR1 is specifically correlated with the phospholipase C–protein kinase C (PKC) pathway, and the Kv2 currents can be modulated by numerous protein kinases, including PKC.[44] Hence, we aimed to confirm that mGluR1 selectively modulated Kv2 current *via* activation of PKC. First, we incubated CCI slices with 10 μM chelerythrine chloride (Che; a PKC inhibitor). The total outward current increased significantly after 10 min of Che incubation and returned nearly to the predrug level after 15 min of aCSF washout (fig. 7A), similar to the effect observed with A841720 treatment. In the presence

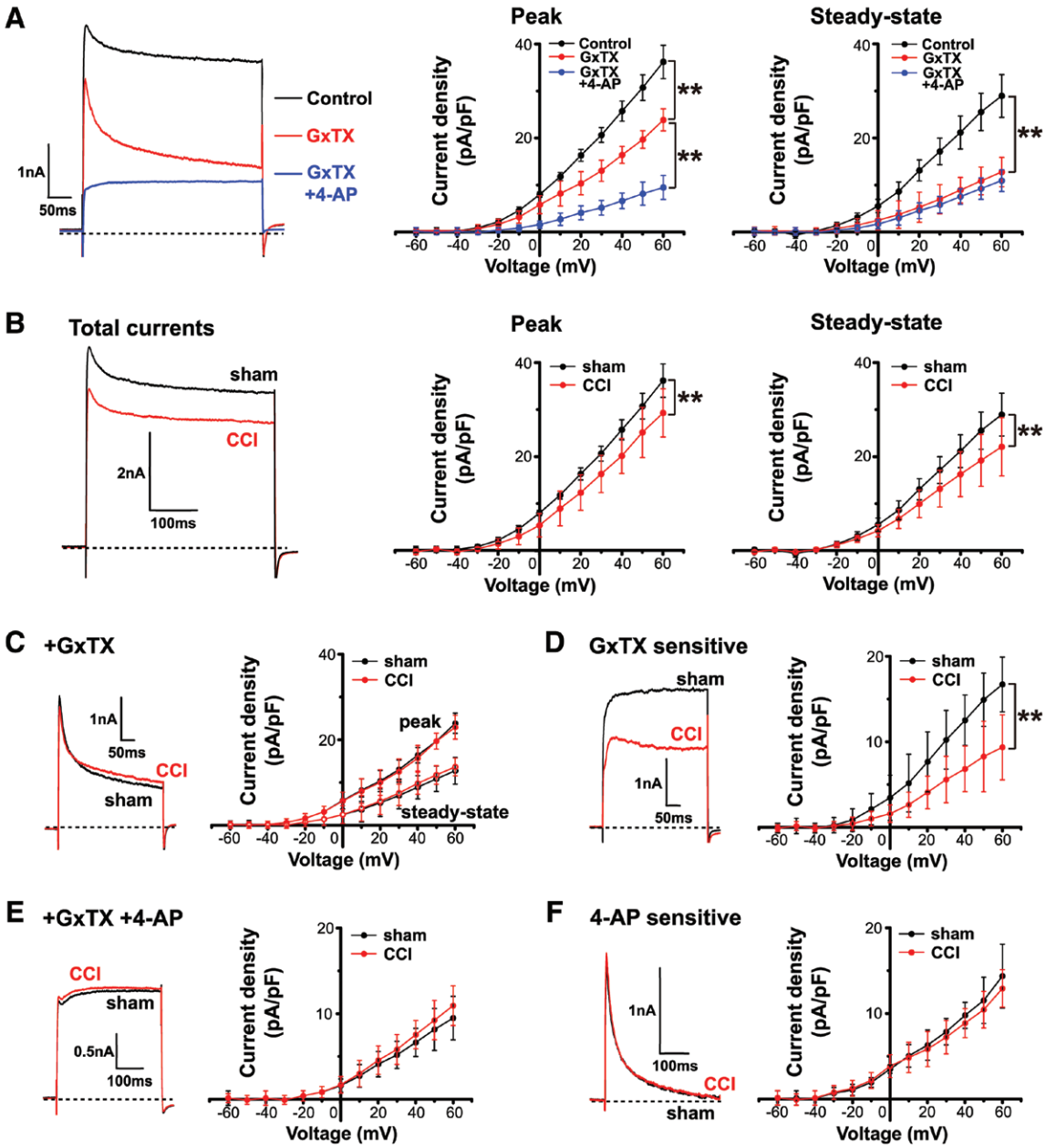

Fig. 5. Voltage-gated potassium channel subunit 2 (Kv2)–mediated guangxitoxin-1E (GxTX)–sensitive potassium current decreases in cholera toxin subunit B (CT-B)+ anterior cingulate cortex (ACC) layer 5 pyramidal neurons (L5 PNs) after chronic constriction injury (CCI). (*A*, *left*) Representative traces show the effects of 100 nM GxTX and 2 mM 4-aminopyridine (4-AP) on total outward current in a CT-B+ ACC L5 PN evoked by voltage step from –90 to +60 mV. (*A*, *middle and right*) Effects of 100 nM GxTX and 2 mM 4-AP on peak and steady-state outward current evoked from –90 mV. Two-way repeated-measures ANOVA and *post hoc* Bonferroni multiple comparison tests, all groups: GxTX and GxTX+4-AP n = 11, control n = 13. (*B*, *left*) Representative traces show the total outward currents in CT-B+ ACC L5 PNs from sham and CCI group evoked by voltage step from –90 mV to +60 mV. (*B*, *middle and right*) The comparison of peak and steady-state outward currents of sham and CCI neurons evoked from –90 mV. Two-way repeated-measures ANOVA, all groups: CCI n = 11, sham n = 13. (*C*) After bath application of 100 nM GxTX, both the peak and steady-state currents are decreased and become identical between sham and CCI neurons. Two-way repeated-measures ANOVA, all groups n = 11. (*D*) The GxTX-sensitive currents are obtained by subtracting the currents after GxTX application (*C*) from the total outward currents (*B*). The GxTX-sensitive currents are compared at steady state and show a significant reduction after CCI. Two-way repeated-measures ANOVA, all groups n = 11. (*E*) After consecutive application of 100 nM GxTX and 2 mM 4-AP, the remaining currents are compared at steady state and are identical between groups. Two-way repeated-measures ANOVA, all groups n = 11. (*F*) The 4-AP-sensitive currents are obtained by subtracting the currents after 4-AP application (*E*) from the currents before 4-AP application (*C*). The 4-AP-sensitive currents are compared at the peak and are also identical between groups. Two-way repeated-measures ANOVA, all groups n = 11. $^{*}P < 0.05$, $^{**}P < 0.01$.

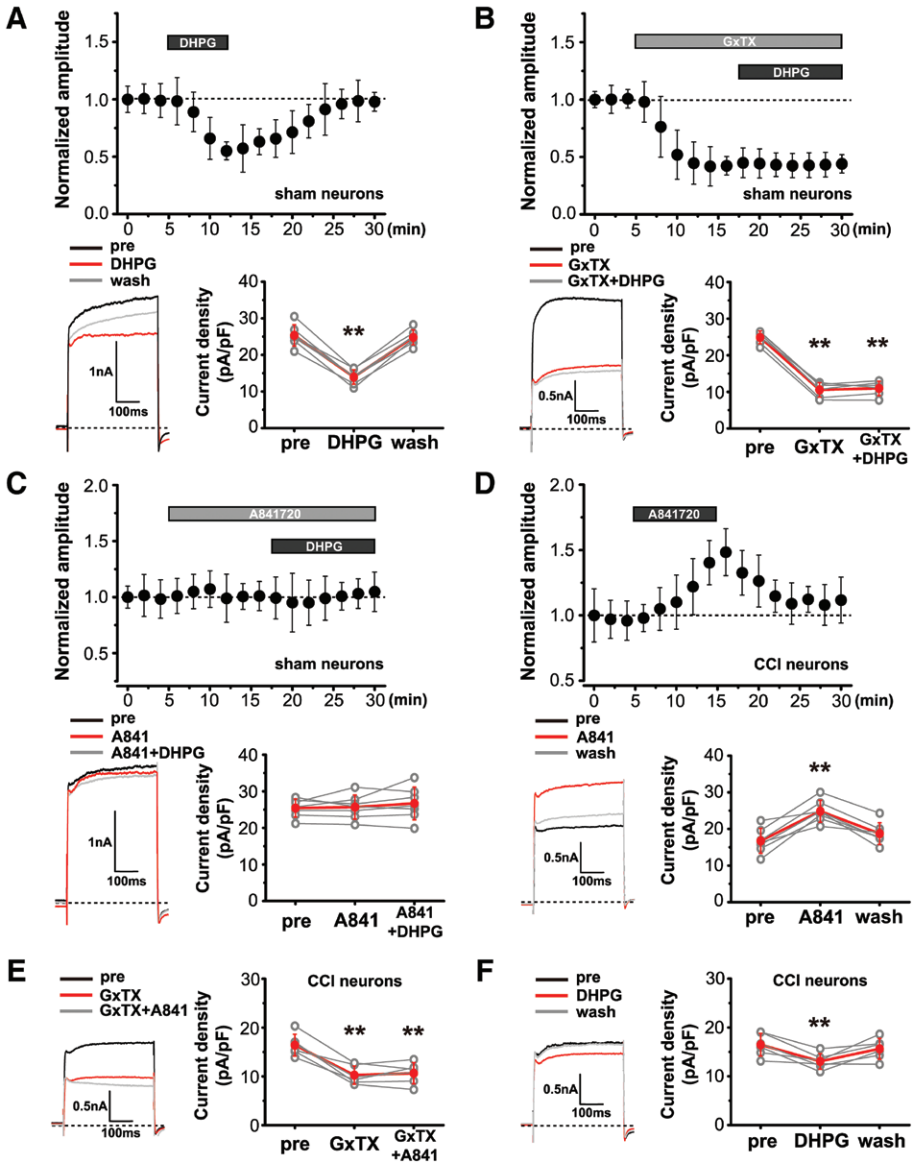

Fig. 6. Inhibition of metabotropic glutamate receptor subtype 1 (mGluR1) rescues the reduced voltage-gated potassium channel subunit 2 (Kv2) current in cholera toxin subunit B (CT-B)+ anterior cingulate cortex (ACC) layer 5 pyramidal neurons (L5 PNs) of chronic constriction injury (CCI) rats. (*A*, *top*) Time course of changes in normalized total outward current amplitudes of sham neurons induced by 15 μM (*RS*)-3,5-dihydroxyphenylglycine (DHPG). The total outward current is evoked by steps from −60 mV to +30 mV in this and the following figures. (*A*, *bottom*) Representative traces of current amplitude at +30 mV (*left*) and comparison of current density (*right*) show a prominent decrease during DHPG application. One-way repeated-measures ANOVA and *post hoc* Bonferroni multiple comparison tests, n = 7; ** *versus* pre. (*B*, *top*) Time course of changes in normalized total outward current amplitudes of sham neurons induced by 15 μM DHPG, in the presence of 100 nM guangxitoxin-1E (GxTX). (*B*, *bottom*) Application of GxTX dramatically decreases the total outward current density, and subsequent additional application of DHPG exerts no effect. One-way repeated-measures ANOVA and *post hoc* Bonferroni multiple comparison tests, n = 6; ** *versus* pre. (*C*, *top*) Time course of changes in normalized total outward current amplitudes of sham neurons induced by 15 μM DHPG, in the presence of 10 μM A841720. (*C*, *bottom*) Application of A841720 has no effect on total outward current density. Subsequent application of DHPG also shows no additional effect. One-way repeated-measures ANOVA and *post hoc* Bonferroni multiple comparison tests, n = 7. A841 represents 9-(dimethylamino)-3-(hexahydro-1*H*-azepin-1-yl)pyrido[3′,2′:4,5]thieno[3,2-*d*]pyrimidin-4(3*H*)-one (A841720) in this figure. (*D*, *top*) Time course of changes in normalized total outward current amplitudes of CCI neurons induced by 10 μM A841720. (*D*, *bottom*) Comparison of current density shows a prominent increase during A841720 application. One-way repeated-measures ANOVA and *post hoc* Bonferroni multiple comparison tests, n = 7; ** *versus* pre. (*E*) After preapplication of 100 nM GxTX, A841720 fails to increase the total outward current density in CCI CT-B+ neurons. One-way repeated-measures ANOVA and *post hoc* Bonferroni multiple comparison tests, n = 6; ** *versus* pre. (*F*) Application of 15 μM DHPG in CCI CT-B+ neurons slightly but significantly reduces the total outward current density. One-way repeated-measures ANOVA and *post hoc* Bonferroni multiple comparison tests, n = 6; ** *versus* pre. *$P < 0.05$, **$P < 0.01$.

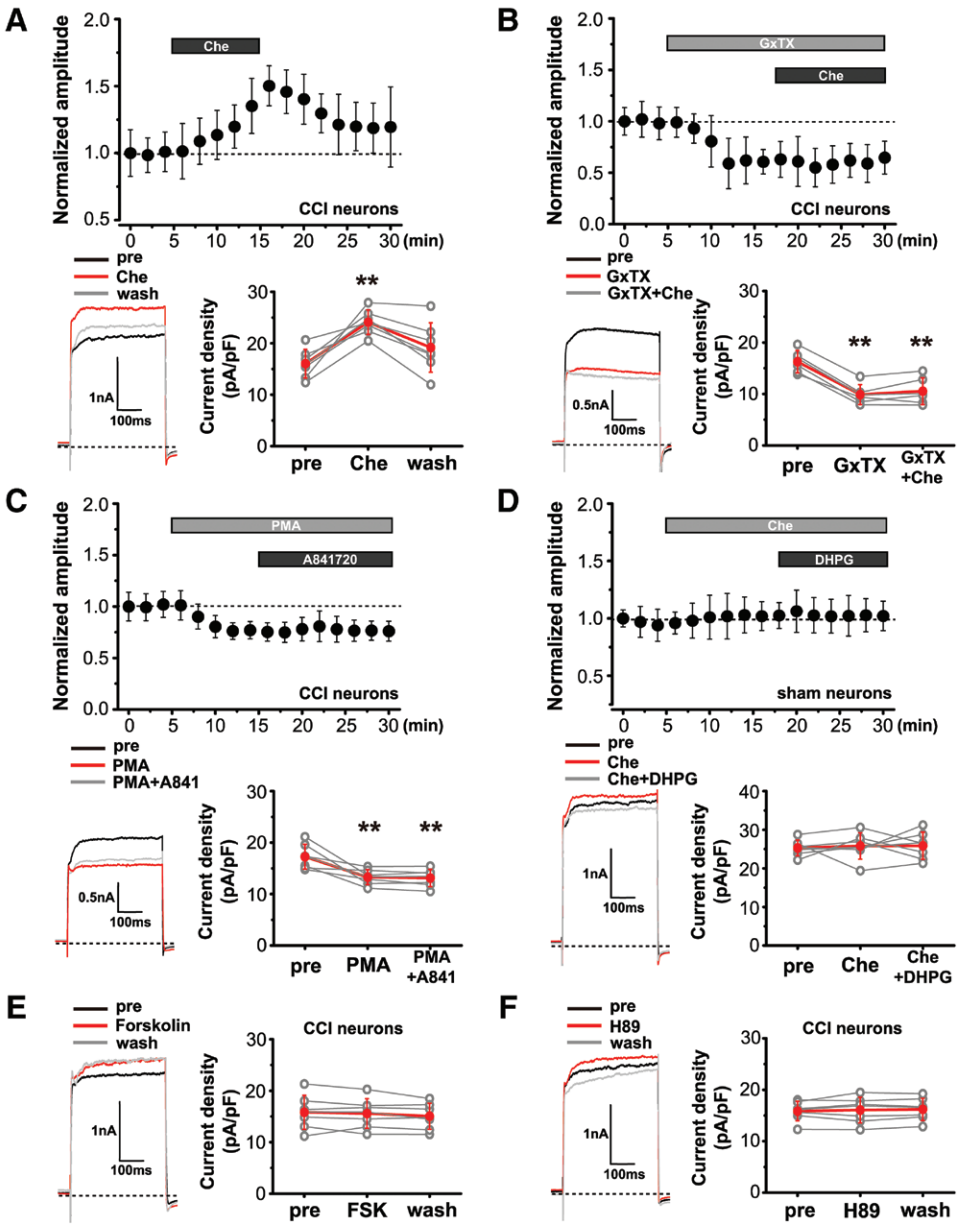

Fig. 7. Metabotropic glutamate receptor subtype 1 (mGluR1) modulates voltage-gated potassium channel subunit 2 (Kv2) current *via* protein kinase C (PKC). (*A*, *top*) Time course of changes in normalized total outward current amplitudes of chronic constriction injury (CCI) neurons induced by 10 μM Che. (*A*, *bottom*) Representative traces of current amplitude at +30 mV (*left*) and comparison of current density (*right*) show a prominent increase during Che application. One-way repeated-measures ANOVA and *post hoc* Bonferroni multiple comparison tests, n = 7; ** *versus* pre. (*B*, *top*) Time course of changes in normalized total outward current amplitudes of CCI neurons induced by 10 μM Che, in the presence of 100 nM guangxitoxin-1E (GxTX). (*B*, *bottom*) Application of GxTX dramatically decreases the total outward current density and subsequent additional application of Che exerts no effect. One-way repeated-measures ANOVA and *post hoc* Bonferroni multiple comparison tests, n = 6; ** *versus* pre. (*C*, *top*) Time course of changes in normalized total outward current amplitudes of CCI neurons induced by 10 μM 9-(dimethylamino)-3-(hexahydro-1*H*-azepin-1-yl)pyrido[3′,2′:4,5]thieno[3,2-*d*]pyrimidin-4(3*H*)-one (A841720), in the presence of 20 μM PMA. (*C*, *bottom*) Application of phorbol 12-myristate 13-acetate (PMA) significantly reduces the total outward current density. Subsequent application of A841720 shows no additional effect. One-way repeated-measures ANOVA and *post hoc* Bonferroni multiple comparison tests, n = 7; ** *versus* pre. (*D*, *top*) Time course of changes in normalized total outward current amplitudes of sham neurons induced by 15 μM (*RS*)-3,5-dihydroxyphenylglycine (DHPG), in the presence of 10 μM Che. (*D*, *bottom*) Application of Che has no effect on total outward current density. Subsequent application of DHPG also shows no additional effect. One-way repeated-measures ANOVA and *post hoc* Bonferroni multiple comparison tests, n = 6. (*E and F*) Neither the application of forskolin (*E*) nor H89 (*F*) rescues the reduced total outward current in CCI cholera toxin subunit B (CT-B)+ neurons. One-way repeated-measures ANOVA, all groups n = 7. *$P < 0.05$, **$P < 0.01$.

of 100 nM GxTX, Che exerted no additional modulation of total outward current (Bonferroni multiple comparison tests: $P = 0.469$, GxTX *vs.* GxTX + Che; fig. 7B), indicating that the effect of Che was indeed mediated by Kv2 channels to a large extent. Then we activated PKC in CCI slices with 20 μM phorbol 12-myristate 3-acetate (PMA; a PKC activator). Bath application of PMA slightly but significantly down-regulated the total outward current (fig. 7C), but, in this condition, additional application of A841720 failed to rescue the Kv2 current (Bonferroni multiple comparison tests: $P = 1.000$, PMA *vs.* PMA + A841720; fig. 7C). Furthermore, we inhibited PKC in sham slices with 10 μM Che but observed no effect on the total outward currents (fig. 7D). However, in this condition, activation of mGluR1 by DHPG failed to down-regulate the Kv2 current (Bonferroni multiple comparison tests: $P = 1.000$, Che *vs.* Che + DHPG; fig. 7D). Both the results in figure 7, C and D, suggest that modulation of Kv2 current by mGluR1 was mediated *via* PKC activity. Furthermore, we observed that neither the activation (fig. 7E) nor inhibition (fig. 7F) of PKA in CCI slices modulated the total outward current of CT-B+ neurons. These results most likely indicate that the group 2 and 3 mGluRs were not involved in the modification of Kv2 current after CCI.

mGluR1 Regulates the Excitability of CT-B+ ACC L5 PNs via an Alteration of Kv2 Current after CCI

Our results thus far showed that there was an inhibition of Kv2 current in CT-B+ ACC L5 PNs caused by the activation of mGluR1 after CCI. Thus, we aimed to determine whether this change was relevant to the decrease in the rate of AP repolarization during burst firing. Measurements of AP number, fAHP, and AP width were performed before and after at least 10 min of 10 μM A841720 bath application with 300-pA depolarizing current elicited APs, in 500 ms duration, in CT-B+ ACC L5 PNs from the sham and CCI groups (fig. 8A). Application of A841720 significantly

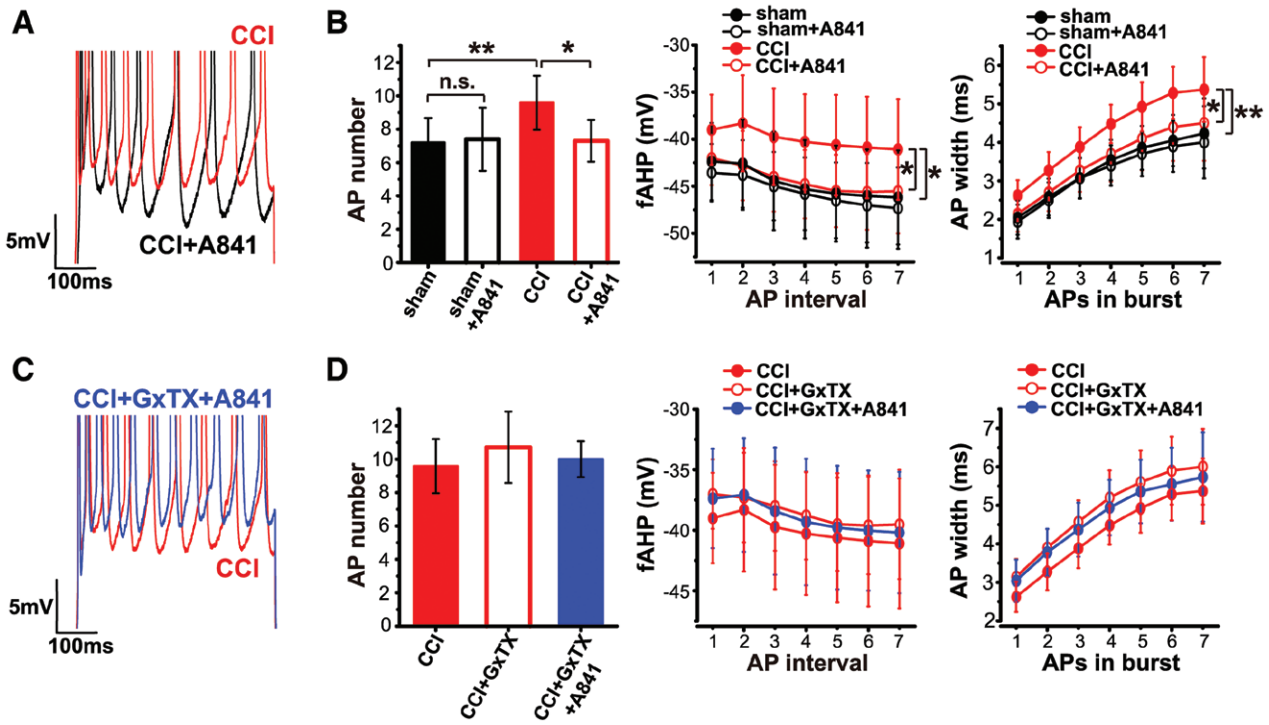

Fig. 8. Inhibition of metabotropic glutamate receptor subtype 1 (mGluR1) attenuates chronic constriction injury (CCI)–induced alterations in firing number, fast afterhyperpolarization (fAHP), and action potential (AP) width *via* disinhibiting voltage-gated potassium channel subunit 2 (Kv2) current. (*A*) Expanded view of the representative traces showing the firing response to a depolarizing current stimulus (+300 pA, 500 ms). (*B*, *left)* AP number of CCI neurons decreases significantly to the sham level after application of 10 μM 9-(dimethylamino)-3-(hexahydro-1*H*-azepin-1-yl)pyrido[3′,2′:4,5]thieno[3,2-*d*]pyrimidin-4(3*H*)-one (A841720). One-way ANOVA and *post hoc* Bonferroni multiple comparison tests, CCI n = 12, all other groups n = 10. (*B*, *middle*) CCI neurons show comparable fAHP potentials to sham neurons after application of 10 μM A841720. Two-way repeated-measures ANOVA and *post hoc* Bonferroni multiple comparison tests, all groups n = 12. (*B*, *right*) CCI neurons also have comparable AP waveforms to sham neurons after application of 10 μM A841720. Two-way repeated-measures ANOVA and *post hoc* Bonferroni multiple comparison tests, all groups n = 12. (*C*) Expanded view of the representative traces showing the firing response to a depolarizing current stimulus (+300 pA, 500 ms). (*D*) After preapplication of 100 nM guangxitoxin-1E (GxTX), the 10 μM A841720 cannot down-regulate the AP number, fAHP potentials, and AP widths of CCI cholera toxin subunit B (CT-B)+ neurons. One-way ANOVA (for AP number) or two-way repeated-measures ANOVA (for fAHP and AP width) and *post hoc* Bonferroni multiple comparison tests, all groups n = 12. n.s. = no significant difference, $^{*}P < 0.05$, $^{**}P < 0.01$.

reduced the number of AP of CCI CT-B+ neurons but had no effect on sham neurons (fig. 8B, left). Moreover, A841720 treatment obviously decreased the fAHP potentials of CCI neurons to sham-like values (fig. 8B, middle). Analysis of AP widths showed a marked decrease in CCI neurons after A841720 application (fig. 8B, right). Neither the fAHP nor the AP width of sham neurons was affected by A841720.

We also tested the hypothesis that the regulation of A841720 on AP repolarization was Kv2 mediated (fig. 8C). We first incubated CCI slices with 100 nM GxTX and observed no significant effect on AP number. However, in the presence of GxTX, additional application of 10 μM A841720 could not down-regulate the AP number of CCI CT-B+ neurons (fig. 8D). Similarly, the regulations of fAHP and AP width in CCI CT-B+ neurons by A841720 were also eliminated with the preapplication of GxTX (fig. 8D).

Kv2 Current in CT-B+ ACC L5 PNs Plays an Important Role in Mediating the Analgesic Effect of mGluR1 Inhibition

Finally, we aimed to test whether the analgesic effect of mGluR1 inhibition was mediated, at least partly, by the reappearance of Kv2 current in the CT-B+ neurons. In the cerebral cortex, Kv2 current is mediated by two kinds of potassium channels. Kv2.1 is expressed nonselectively in all of the L5 PNs, whereas Kv2.2 is mainly expressed in the contralateral-projecting neurons.[38] We confirmed this expression pattern in the ACC (fig. 9A). Moreover, PKCs selectively regulate Kv2.2 but not Kv2.1.[44] Thus, lentivirus expressing specific shRNA (Kv2.2 shRNA) was bilaterally injected into the ACC to selectively knock down Kv2 current in CT-B+ neurons, and the CCI rats that received nontargeting shNC injection were used as controls (fig. 9B). Western blot analyses showed that Kv2.2 expression was successfully suppressed 7 days after Kv2.2 shRNA injection, and this suppression persisted for more than 1 week (fig. 9C).

Next, we evaluated the effect of several manipulations on paw-withdrawal thermal latency and mechanical threshold of the injured hind paw. Knockdown of Kv2.2 in ACC L5 did not alter the thermal and mechanical threshold of rats in either the sham or CCI group on day 7 after surgery (fig. 9D). Microinjection of A841720 at the same site nearly completely attenuated thermal hyperalgesia and also significantly alleviated mechanical allodynia in CCI rats on day 7 after surgery (fig. 9E). This analgesic effect appeared rapidly within 30 min and decayed back to the sensitized condition within 120 min, consistent with the diffusion of the drug from the site of action. However, in the CCI rats, which had been infused with Kv2.2-shRNA, the analgesic effect of A841720 was significantly reduced (Bonferroni multiple comparison tests: thermal latency: $P = 0.021$, mechanical threshold: $P = 0.031$, CCI + A841720 *vs.* shRNA + CCI + A841720; fig. 9E), suggesting that this analgesic effect might be at least partly mediated by Kv2.2 channels on CT-B+ ACC L5 PNs.

Discussion

In the present study, we provided strong evidence that L5 PNs in the ACC, as in the mPFC, had a subtype projecting to the contralateral cortex and exhibiting few HCN1 channels. In this study, this subtype was named CT-B+ neurons, and these neurons also became hyperexcitable after peripheral nerve injury. Furthermore, we revealed that the Kv2 currents of these neurons were down-regulated after CCI. Inhibition of mGluR1 effectively rescued the decreased Kv2 current and attenuated the spike hyperactivity. In addition, knockdown of the Kv2 current in CT-B+ ACC L5 PNs attenuated the analgesic effect of mGluR1 inhibition.

Projection-specific Alteration of L5 PNs in the ACC after CCI

L5 PNs in several neocortical regions have been shown to have distinct morphology and physiology depending on their long-range projection target.[38,45–47] Our present study expands this pattern to the rostral rat ACC, which is closely related to the emotional response and sensory perception of chronic pain. It has been proposed that L5 PNs in the mPFC can be segregated into two classes, those projecting to the contralateral cortex (named commissural[9] neurons or intratelencephalic[48] neurons) and those with projections outside of the telencephalon (named corticopontine neurons or pyramidal tract neurons). We confirmed that the L5 PNs in ACC also had a subtype projecting to the contralateral cortex (CT-B+ neurons), which showed distinct electrophysiology relative to the CT-B– neurons. The CT-B+ neurons had obviously greater input resistance and adaptation ratio than the CT-B– neurons, consistent with the observations of commissural and corticopontine neurons in mPFC.[8,9] More importantly, the CT-B+ neurons displayed much smaller sag ratios than CT-B– neurons and expressed fewer HCN1 channels, similar to the report in the mPFC that the expression of HCN1 mRNA was less in intratelencephalic compared with pyramidal tract neurons.[20] This finding may be one of the potential reasons accounting for the distinct membrane properties of CT-B+/commissural/intratelencephalic compared with CT-B–/corticopontine/pyramidal tract neurons.

Numerous studies have investigated the alterations of synaptic transmission in layer 5 of ACC after peripheral nerve injury,[49,50] without distinguishing the difference between neuronal subtypes. Santello and Nevian[6] have shown that the enhancement of dendritic integration by I_h reduction after sciatic nerve injury increased the excitability of ACC L5 PNs. Although they did not clearly indicate which neuronal subtype was tested, it is conceivable that, in their study, the L5 PNs refer to the corticopontine neurons, because these neurons exhibited a considerable number of HCN1 channels and an increasing gradient of dendritic sag ratio with distance from the soma. Our previous study[7] also showed that the I_h reduction resulted in hyperexcitability of CT-B– ACC L5 PNs after CCI, additionally confirming that the CT-B– neurons might be corticopontine neurons.

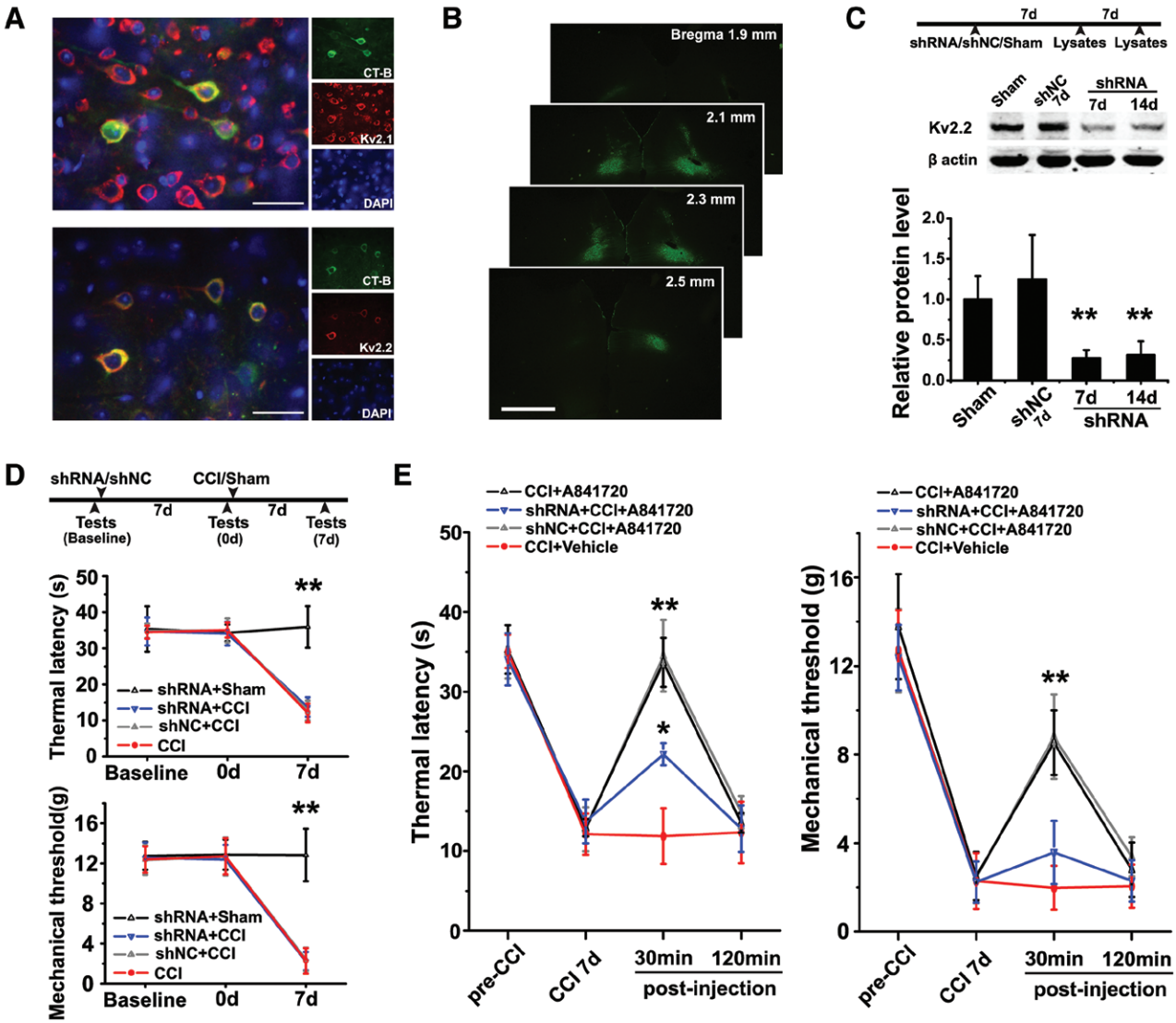

Fig. 9. Knockdown of voltage-gated potassium channel subunit 2 (Kv2) current in the cholera toxin subunit B (CT-B)+ anterior cingulate cortex (ACC) layer 5 pyramidal neurons (L5 PNs) partly attenuates the analgesic effect of metabotropic glutamate receptor subtype 1 (mGluR1) inhibition. (*A*) Magnified images showing CT-B and Kv2.1 (*top*) or CT-B and Kv2.2 (*bottom*) double labeling in the left ACC L5. The CT-B is injected into the right ACC. *Scale bar* = 50 μm. (*B*) Representative immunofluorescence images showing the efficiency of lentivirus transfection in the ACC on day 7 after the injection. *Scale bar* = 1,000 μm. (*C*) Western blots showing successful suppression of Kv2.2 in the ACC on days 7 and 14 after short hairpin RNA (shRNA)–lentivirus injection. The negative control shRNA (shNC; nontargeting shRNA) has no effect. One-way ANOVA and *post hoc* Bonferroni multiple comparison tests, all groups n = 6 rats; ** *versus* sham. (*C, top*) A schematic of the Western blotting experimental design. (*D*, *top*) A schematic of the behavioral testing protocol. Neither intra-ACC Kv2.2-shRNA nor shNC has a significant effect on chronic constriction injury (CCI)–induced thermal hyperalgesia (*middle*) and mechanical allodynia (*bottom*). Two-way repeated-measures ANOVA and *post hoc* Bonferroni multiple comparison tests, all groups n = 6 rats; ** *versus* CCI. (*E*) Intra-ACC microinjection of 9-(dimethylamino)-3-(hexahydro-1*H*-azepin-1-yl)pyrido[3′,2′:4,5]thieno[3,2-*d*]pyrimidin-4(3*H*)-one (A841720; day 7 post-CCI) produces significant analgesic effects. However, in the rats that had been infused with Kv2.2-shRNA before CCI surgery, A841720 partly loses its ability to alleviate thermal hyperalgesia (*left*) and nearly completely fails to alleviate mechanical allodynia (*right*). Preinfusion of shNC does not change the effect of A841720. Two-way repeated-measures ANOVA and *post hoc* Bonferroni multiple comparison tests, all groups n = 6 rats; *,** *versus* CCI + vehicle. *$P < 0.05$, **$P < 0.01$.

Likewise, in the present study, we observed a significant up-regulation of excitability of CT-B+ ACC L5 PNs after CCI. However, the increased firing frequency of CT-B+ neurons was observed around the steady state (fig. 3C) of 500-ms depolarizing current stimulus, which differed with that of CT-B– neurons observed around the onset,[7] suggesting that the CT-B+ neurons adapted more slowly to steady-state frequency after CCI. In addition, we observed that the sag ratios of CT-B+ neurons were unaltered on day 7 after CCI during somatic recording. Given that the I_h properties

of CT-B+/commissural/intratelencephalic neurons are relatively uniform across the extent of the apical dendrite,[51] dendritic recordings most likely will not find any changes in sag ratios after CCI, which is inconsistent with the observation in corticopontine dendrites. Thus, it is conceivable that other modifications rather than I_h reduction lead to the hyperexcitability of CT-B+ ACC L5 PNs after CCI.

Role of Kv2 Channels in ACC Hyperexcitability

The CCI-induced increase in AP width and fAHP potential observed in our study have the potential to increase the number of APs during burst firing by shortening the subsequent depolarization to spike threshold.[28,52] It has been shown in dopaminergic neurons in the substantia nigra that Kv2 channels are activated sufficiently rapidly during APs, and the acceleration of firing rate after Kv2 inhibition is straightforward, from the loss of a relatively long-lasting hyperpolarizing effect during the late falling phase and AHP of the spike.[28] Consistent with this finding, we observed a significant reduction in the amplitude of Kv2-mediated, GxTX-sensitive current after CCI, and rescue of the Kv2 current by inhibiting mGluR1 successfully decreased the spike number of CCI neurons. In addition, the increased propensity of CCI CT-B+ neurons to enter the depolarization block was also a main effect of Kv2 reduction,[28,41] resulting in an inactivation of sodium channels as a consequence of the more depolarized interspike potential. The increased inactivation of sodium channels will intuitively result in fewer spikes[53] during larger depolarization stimuli (greater than 400 pA in the present study). However, during the weaker and perhaps physiologically more pertinent stimuli, the reduced recovery from inactivation of sodium channels may be relatively less severe because the maximum dV/dt of APs was comparable between the sham and CCI neurons. Therefore, the effect that the reduced Kv2 current has on firing property is likely influenced by the details of the sodium channels on the neuron.[41]

In addition to the Kv2 channel, A-type K^+ channels also play a role in AP repolarization.[54,55] Neurons with decreased A-type channel expression have smaller fAHPs and broader APs.[29] However, we did not observe any change in the 4-AP–sensitive A-type current after CCI. Moreover, although we did not examine whether other conductances, such as Kv7-mediated M-type current and BK-type Ca^{2+}-activated K^+ current, were changed after CCI, the residual current after GxTX and 4-AP application was unaltered. Thus, despite the intricate composition of the residual current, its overall effect may not contribute to the reduction of total outward current after CCI. However, it can be difficult to interpret the functional effect of removing a given conductance, because the activation of other conductances can change.[28] Taken together, our results suggest that the Kv2 channel is one of the key elements contributing to the changes in spike repolarization during bursts after CCI. However, the analgesic strategy directly targeting potassium channels should identify the full range of interactions among the many conductances that could potentially participate in the CCI-induced changes of neuronal excitability.

Projection-specific Modulation of Cortical Excitation by mGluR1 Inhibition

Alteration of mGluR1 at the cortical level is an important pathologic change for sustained nociceptive hypersensitivity.[7,56] However, studies examining whether activation of mGluR1 in the ACC has a cell type-specific effect are, to our knowledge, lacking after CCI. In the CT-B– neurons, activation of mGluR1 excited these neurons by inhibiting I_h.[7] However, the effect of mGluR1 activation on CT-B+ neurons, if any, appears to involve a different mechanism, because these neurons exhibit little I_h.

In the present study, we confirmed that inhibiting mGluR1 rescued the suppressed Kv2 current density and thus decreased the excitability of CT-B+ neurons in CCI slices. This effect was mimicked by a PKC inhibitor and blocked by a PKC activator. We therefore speculated that activation of mGluR1 excessively activated PKC and consequently inhibited Kv2 currents, thereby inducing or facilitating neuronal hyperexcitability in CT-B+ ACC L5 PNs after CCI. Other neurotransmitter systems that activate PKC could have similar effects. The mGluR5, the other subtype of group 1 mGluRs, might exhibited a very small effect on the alterations stated above, because the application of A841720 nearly entirely blocked the effect of DHPG. However, we cannot exclude the possibility that both mGluR1 and mGluR5 are necessary for the effect of DHPG. Our results also suggested that activation of mGluR1 after CCI excites both CT-B– and CT-B+ neurons but through distinct pathways. Reduction of I_h is restricted to CT-B– neurons, because the sag ratio of CT-B+ neurons was unaltered. Similarly, the down-regulation of Kv2 current by PKC could only be observed in CT-B+ neurons, because the PKC modifies Kv2.2 but not Kv2.1,[44] and Kv2.2 is mainly expressed on CT-B+/intratelencephalic neurons.[38] Moreover, we provided evidence that the analgesic effect of mGluR1 inhibition was at least partly mediated by the Kv2 current in CT-B+ ACC L5 PNs, because this effect was significantly attenuated by preknockdown of Kv2.2.

In summary, we provide direct evidence to support that ACC L5 PNs have a subtype projecting to the contralateral cortex. These neurons become hyperexcitable after peripheral nerve injury, resulting from an inhibition of Kv2 current but not I_h. Activation of mGluR1 and subsequent activation of PKC are important causes of the inhibition observed in the Kv2 current. Conceivably, CT-B+ neurons adapt more slowly to fire persistently, which affects their ability to synchronize with the surrounding network.[57,58] Corticopontine/pyramidal tract/CT-B– neurons receive inputs from both corticopontine and commissural neurons, whereas commissural/intratelencephalic/CT-B+ neurons receive inputs from other commissural neurons but very infrequently from

corticopontine neurons.[11] The unidirectional commissural to corticopontine connectivity might make corticopontine/CT-B– neurons a final convergence point for numerous local synaptic inputs.[59] Therefore, hyperexcited CT-B+ neurons after CCI may additionally contribute to the overexcitation of CT-B– neurons, and inhibition of mGluR1 in the ACC L5 will exert an analgesic effect through these two aspects.

Acknowledgments

The authors are very grateful to Prof. Peng-Hui Chen (Department of Neurobiology, Third Military Medical University, Chongqing, China) for the technique assistance in whole cell clamp recording.

Research Support

Supported by the National Natural Science Foundation of China (grant No. 31171069).

Competing Interests

The authors declare no competing interests.

Correspondence

Address correspondence to Dr. Ruan: Department of Neurobiology, College of Basic Medical Science, Chongqing Key Laboratory of Neurobiology, Third Military Medical University, No. 30, Gaotanyan Street, Shapingba District, Chongqing 400038, China. hzruan163@163.com.

References

1. Apkarian AV, Baliki MN, Geha PY: Towards a theory of chronic pain. Prog Neurobiol 2009; 87:81–97
2. Apkarian AV, Bushnell MC, Treede RD, Zubieta JK: Human brain mechanisms of pain perception and regulation in health and disease. Eur J Pain 2005; 9:463–84
3. Vogt BA: Pain and emotion interactions in subregions of the cingulate gyrus. Nat Rev Neurosci 2005; 6:533–44
4. Shackman AJ, Salomons TV, Slagter HA, Fox AS, Winter JJ, Davidson RJ: The integration of negative affect, pain and cognitive control in the cingulate cortex. Nat Rev Neurosci 2011; 12:154–67
5. Wager TD, Atlas LY, Lindquist MA, Roy M, Woo CW, Kross E: An fMRI-based neurologic signature of physical pain. N Engl J Med 2013; 368:1388–97
6. Santello M, Nevian T: Dysfunction of cortical dendritic integration in neuropathic pain reversed by serotoninergic neuromodulation. Neuron 2015; 86:233–46
7. Gao SH, Wen HZ, Shen LL, Zhao YD, Ruan HZ: Activation of mGluR1 contributes to neuronal hyperexcitability in the rat anterior cingulate cortex via inhibition of HCN channels. Neuropharmacology 2016; 105:361–77
8. van Aerde KI, Feldmeyer D: Morphological and physiological characterization of pyramidal neuron subtypes in rat medial prefrontal cortex. Cereb Cortex 2015; 25:788–805
9. Dembrow NC, Chitwood RA, Johnston D: Projection-specific neuromodulation of medial prefrontal cortex neurons. J Neurosci 2010; 30:16922–37
10. Wang Y, Markram H, Goodman PH, Berger TK, Ma J, Goldman-Rakic PS: Heterogeneity in the pyramidal network of the medial prefrontal cortex. Nat Neurosci 2006; 9:534–42
11. Shepherd GM: Corticostriatal connectivity and its role in disease. Nat Rev Neurosci 2013; 14:278–91
12. Zhuo M: Cortical excitation and chronic pain. Trends Neurosci 2008; 31:199–207
13. Bennett CE, Burnett DA, Greenlee WJ, Knutson CE, Korakas P, Li C, Tulshian D, Wu WL, Bertorelli R, Fredduzzi S, Grilli M, Lozza G, Reggiani A, Veltri A: Fused tricyclic mGluR1 antagonists for the treatment of neuropathic pain. Bioorg Med Chem Lett 2012; 22:1575–8
14. Lüscher C, Huber KM: Group 1 mGluR-dependent synaptic long-term depression: mechanisms and implications for circuitry and disease. Neuron 2010; 65:445–59
15. Noda K, Anzai T, Ogata M, Akita H, Ogura T, Saji M: Antisense knockdown of spinal-mGluR1 reduces the sustained phase of formalin-induced nociceptive responses. Brain Res 2003; 987:194–200
16. Chiechio S, Nicoletti F: Metabotropic glutamate receptors and the control of chronic pain. Curr Opin Pharmacol 2012; 12:28–34
17. Chiechio S: Modulation of chronic pain by metabotropic glutamate receptors. Adv Pharmacol 2016; 75:63–89
18. Seong HJ, Carter AG: D1 receptor modulation of action potential firing in a subpopulation of layer 5 pyramidal neurons in the prefrontal cortex. J Neurosci 2012; 32:10516–21
19. Avesar D, Gulledge AT: Selective serotonergic excitation of callosal projection neurons. Front Neural Circuits 2012; 6:12
20. Sheets PL, Suter BA, Kiritani T, Chan CS, Surmeier DJ, Shepherd GM: Corticospinal-specific HCN expression in mouse motor cortex: I(h)-dependent synaptic integration as a candidate microcircuit mechanism involved in motor control. J Neurophysiol 2011; 106:2216–31
21. He WJ, Cui J, Du L, Zhao YD, Burnstock G, Zhou HD, Ruan HZ: Spinal P2X(7) receptor mediates microglia activation-induced neuropathic pain in the sciatic nerve injury rat model. Behav Brain Res 2012; 226:163–70
22. Bennett GJ, Xie YK: A peripheral mononeuropathy in rat that produces disorders of pain sensation like those seen in man. Pain 1988; 33:87–107
23. Zimmermann M: Ethical guidelines for investigations of experimental pain in conscious animals. Pain 1983; 16:109–10
24. Paxinos G, Watson C: The rat brain in stereotaxic coordinates. New York, Academic, 1998
25. Gabbott PL, Dickie BG, Vaid RR, Headlam AJ, Bacon SJ: Local-circuit neurones in the medial prefrontal cortex (areas 25, 32 and 24b) in the rat: morphology and quantitative distribution. J Comp Neurol 1997; 377:465–99
26. Han M, Xiao X, Yang Y, Huang RY, Cao H, Zhao ZQ, Zhang YQ: SIP30 is required for neuropathic pain-evoked aversion in rats. J Neurosci 2014; 34:346–55
27. Brown JT, Chin J, Leiser SC, Pangalos MN, Randall AD: Altered intrinsic neuronal excitability and reduced Na+ currents in a mouse model of Alzheimer's disease. Neurobiol Aging 2011; 32:2109.e1–14
28. Kimm T, Khaliq ZM, Bean BP: Differential regulation of action potential shape and burst-frequency firing by BK and Kv2 channels in substantia nigra dopaminergic neurons. J Neurosci 2015; 35:16404–17
29. Simkin D, Hattori S, Ybarra N, Musial TF, Buss EW, Richter H, Oh MM, Nicholson DA, Disterhoft JF: Aging-related hyperexcitability in CA3 pyramidal neurons is mediated by enhanced A-type K+ channel function and expression. J Neurosci 2015; 35:13206–18
30. Hargreaves K, Dubner R, Brown F, Flores C, Joris J: A new and sensitive method for measuring thermal nociception in cutaneous hyperalgesia. Pain 1988; 32:77–88

31. Chaplan SR, Bach FW, Pogrel JW, Chung JM, Yaksh TL: Quantitative assessment of tactile allodynia in the rat paw. J Neurosci Methods 1994; 53:55–63
32. He C, Luo F, Chen X, Chen F, Li C, Ren S, Qiao Q, Zhang J, de Lecea L, Gao D, Hu Z: Superficial layer-specific histaminergic modulation of medial entorhinal cortex required for spatial learning. Cereb Cortex 2016; 26:1590–608
33. Chiou CS, Chen CC, Tsai TC, Huang CC, Chou D, Hsu KS: Alleviating bone cancer-induced mechanical hypersensitivity by inhibiting neuronal activity in the anterior cingulate cortex. Anesthesiology 2016; 125:779–92
34. Xu W, Südhof TC: A neural circuit for memory specificity and generalization. Science 2013; 339:1290–5
35. Gee S, Ellwood I, Patel T, Luongo F, Deisseroth K, Sohal VS: Synaptic activity unmasks dopamine D2 receptor modulation of a specific class of layer V pyramidal neurons in prefrontal cortex. J Neurosci 2012; 32:4959–71
36. Disterhoft JF, Oh MM: Alterations in intrinsic neuronal excitability during normal aging. Aging Cell 2007; 6:327–36
37. Wu WW, Chan CS, Disterhoft JF: Slow afterhyperpolarization governs the development of NMDA receptor-dependent afterdepolarization in CA1 pyramidal neurons during synaptic stimulation. J Neurophysiol 2004; 92:2346–56
38. Bishop HI, Guan D, Bocksteins E, Parajuli LK, Murray KD, Cobb MM, Misonou H, Zito K, Foehring RC, Trimmer JS: Distinct cell- and layer-specific expression patterns and independent regulation of Kv2 channel subtypes in cortical pyramidal neurons. J Neurosci 2015; 35:14922–42
39. Hwang PM, Fotuhi M, Bredt DS, Cunningham AM, Snyder SH: Contrasting immunohistochemical localizations in rat brain of two novel K+ channels of the Shab subfamily. J Neurosci 1993; 13:1569–76
40. Trimmer JS: Immunological identification and characterization of a delayed rectifier K+ channel polypeptide in rat brain. Proc Natl Acad Sci USA 1991; 88:10764–8
41. Liu PW, Bean BP: Kv2 channel regulation of action potential repolarization and firing patterns in superior cervical ganglion neurons and hippocampal CA1 pyramidal neurons. J Neurosci 2014; 34:4991–5002
42. Malin SA, Nerbonne JM: Delayed rectifier K+ currents, IK, are encoded by Kv2 alpha-subunits and regulate tonic firing in mammalian sympathetic neurons. J Neurosci 2002; 22:10094–105
43. Murakoshi H, Trimmer JS: Identification of the Kv2.1 K+ channel as a major component of the delayed rectifier K+ current in rat hippocampal neurons. J Neurosci 1999; 19:1728–35
44. Dong WH, Chen JC, He YL, Xu JJ, Mei YA: Resveratrol inhibits K(v)2.2 currents through the estrogen receptor GPR30-mediated PKC pathway. Am J Physiol Cell Physiol 2013; 305:C547–57
45. Brown SP, Hestrin S: Intracortical circuits of pyramidal neurons reflect their long-range axonal targets. Nature 2009; 457:1133–6
46. Morishima M, Kawaguchi Y: Recurrent connection patterns of corticostriatal pyramidal cells in frontal cortex. J Neurosci 2006; 26:4394–405
47. Molnár Z, Cheung AF: Towards the classification of subpopulations of layer V pyramidal projection neurons. Neurosci Res 2006; 55:105–15
48. Reiner A, Hart NM, Lei W, Deng Y: Corticostriatal projection neurons: Dichotomous types and dichotomous functions. Front Neuroanat 2010; 4:142
49. Chen T, Koga K, Descalzi G, Qiu S, Wang J, Zhang LS, Zhang ZJ, He XB, Qin X, Xu FQ, Hu J, Wei F, Huganir RL, Li YQ, Zhuo M: Postsynaptic potentiation of corticospinal projecting neurons in the anterior cingulate cortex after nerve injury. Mol Pain 2014; 10:33
50. Blom SM, Pfister JP, Santello M, Senn W, Nevian T: Nerve injury-induced neuropathic pain causes disinhibition of the anterior cingulate cortex. J Neurosci 2014; 34:5754–64
51. Kalmbach BE, Chitwood RA, Dembrow NC, Johnston D: Dendritic generation of mGluR-mediated slow afterdepolarization in layer 5 neurons of prefrontal cortex. J Neurosci 2013; 33:13518–32
52. Marcantoni A, Raymond EF, Carbone E, Marie H: Firing properties of entorhinal cortex neurons and early alterations in an Alzheimer's disease transgenic model. Pflugers Arch 2014; 466:1437–50
53. Guan D, Armstrong WE, Foehring RC: Kv2 channels regulate firing rate in pyramidal neurons from rat sensorimotor cortex. J Physiol 2013; 591:4807–25
54. Kim J, Wei DS, Hoffman DA: Kv4 potassium channel subunits control action potential repolarization and frequency-dependent broadening in rat hippocampal CA1 pyramidal neurones. J Physiol 2005; 569(pt 1):41–57
55. Zhang L, McBain CJ: Potassium conductances underlying repolarization and after-hyperpolarization in rat CA1 hippocampal interneurones. J Physiol 1995; 488 (pt 3):661–72
56. Kang SJ, Liu MG, Chen T, Ko HG, Baek GC, Lee HR, Lee K, Collingridge GL, Kaang BK, Zhuo M: Plasticity of metabotropic glutamate receptor-dependent long-term depression in the anterior cingulate cortex after amputation. J Neurosci 2012; 32:11318–29
57. Ladenbauer J, Augustin M, Shiau L, Obermayer K: Impact of adaptation currents on synchronization of coupled exponential integrate-and-fire neurons. PLoS Comput Biol 2012; 8:e1002478
58. Fuhrmann G, Markram H, Tsodyks M: Spike frequency adaptation and neocortical rhythms. J Neurophysiol 2002; 88:761–70
59. Dembrow N, Johnston D: Subcircuit-specific neuromodulation in the prefrontal cortex. Front Neural Circuits 2014; 8:54